Colloquium: Cavity-enhanced quantum network nodes

Andreas Reiserer*

Max-Planck-Institut für Quantenoptik,
Hans-Kopfermann-Strasse 1, D-85748 Garching, Germany
and Technical University of Munich, TUM School of Natural Sciences
and Munich Center for Quantum Science and Technology (MCQST),
James-Franck-Strasse 1, D-85748 Garching, Germany

(published 16 December 2022)

A future quantum network will consist of quantum processors that are connected by quantum channels, just like conventional computers are wired up to form the Internet. In contrast to classical devices, however, the entanglement and nonlocal correlations available in a quantum-controlled system facilitate novel fundamental tests of quantum theory. In addition, they enable numerous applications in distributed quantum information processing, quantum communication, and precision measurement. While pioneering experiments have demonstrated the entanglement of two quantum nodes separated by up to 1.3 km, and three nodes in the same laboratory, accessing the full potential of quantum networks requires scaling of these prototypes to many more nodes and global distances. This is an outstanding challenge, posing high demands on qubit control fidelity, qubit coherence time, and coupling efficiency between stationary and flying qubits. This Colloquium describes how optical resonators facilitate quantum network nodes that achieve the aforementioned prerequisites in different physical systems (trapped atoms, defect centers in wide-band-gap semiconductors, and rare-earth dopants) by enabling high-fidelity qubit initialization and readout, efficient generation of qubit-photon and remote qubit-qubit entanglement, and quantum gates between stationary and flying qubits. These advances open a realistic perspective toward the implementation of global-scale quantum networks in the near future.

DOI: 10.1103/RevModPhys.94.041003

CONTENTS

I. INTRODUCTION

The field of quantum technology aims at harnessing the strangeness and the power of quantum mechanics in order to implement devices that provide functionalities that are unattainable for any classical machine. In recent decades, four main fields of applications have been identified: The first is quantum communication (Gisin and Thew, 2007; Ekert and Renner, 2014), which allows for provably secure encryption and authentication without any assumptions about the capabilities of an adversary. The second field is quantum computation (Preskill, 2018), which can fundamentally increase the size or speed upon solving specific computational tasks. The third field is quantum simulation (Georgescu, Ashhab, and Nori, 2014), in which complex and inaccessible quantum systems are emulated on a device that is more accessible, with the aim of gaining a better understanding and of eventually guiding the development of new materials and drugs. The final field is quantum sensing (Degen, Reinhard, and Cappellaro, 2017), which can improve the resolution or sensitivity of the measurement of many quantities.

These applications have vastly different requirements with respect to the isolation, coherence, and techniques to control the used quantum system. Therefore, specialized hardware is often employed. As an example, optical photons facilitate the distribution of quantum states at the fastest possible speed, the speed of light. Furthermore, they can be coupled into optical fibers and transmitted with negligible decoherence over many kilometers before they get absorbed. Finally, since photons do not interact, they can be multiplexed to the same channel to achieve higher rates. The aforementioned properties make photons ideally suited for quantum communication (Gisin and Thew, 2007; Ekert and Renner, 2014) but are a severe disadvantage for all applications that require quantum information to be kept over longer times, or qubits to interact with one another or with external fields. This includes sensors of stationary fields (Degen, Reinhard, and Cappellaro, 2017), as

*andreas.reiserer@tum.de

well as processors and memory elements of a quantum computer (Preskill, 2018). Therefore, for the latter tasks other physical systems seem favorable. Most prominently, the spin of atoms in vacuum, or impurities and dopants in certain solids, offers unrivaled coherence time. The isolation required for such long-term memory impedes the efficient and controlled coupling between qubits, as required for information processing.

In a hybrid system of light and matter qubits, forming a quantum network (Duan and Monroe, 2010; Reiserer and Rempe, 2015) or "quantum internet" (Kimble, 2008; Wehner, Elkouss, and Hanson, 2018), one can achieve the aforementioned contradicting requirements of implementing a controlled coupling between qubits while isolating them from the environment. The realization of such a quantum network may thus be an enabling technology for applications in all fields of quantum science: In quantum communication, entanglement-assisted communication can ensure unbreakable encryption (Ekert and Renner, 2014) and facilitate other important tasks such as authentication, position verification, secret sharing, voting, and compression (Buhrman *et al.*, 2010; Wehner, Elkouss, and Hanson, 2018). In addition, a network of distributed quantum sensors may measure time (Kómár *et al.*, 2014), magnetic fields, gravity, or starlight (Gottesman, Jennewein, and Croke, 2012; Khabiboulline *et al.*, 2019) with unprecedented sensitivity or resolution (Proctor, Knott, and Dunningham, 2018). Furthermore, in quantum computing and simulation a modular architecture may improve scalability (Awschalom *et al.*, 2013; Monroe and Kim, 2013; Kinos *et al.*, 2021) by connecting smaller processing units via photons. In such remote systems, one can avoid crosstalk and correlated errors that can be difficult to correct (Lidar and Brun, 2013). Finally, quantum networks may allow users with finite quantum capabilities to perform computations on a remote quantum supercomputer (Barz *et al.*, 2012; Fitzsimons, 2017).

In addition to the known applications, novel possibilities of unforeseeable impact may emerge once global quantum networks become available. This puts the realization of a scalable quantum network at the forefront of today's quantum science.

In this context, scalability means that adding another entangled node or increasing the distance between the nodes will add technical complexity and require additional resources but will not be hindered by fundamental restrictions. In current physical systems, however, there are two fundamental restrictions that have to be overcome: absorption that is unavoidable in any quantum channel and errors caused by decoherence and control imperfections.

The former is the major challenge for scaling to larger distances: Consider an optical fiber link between distant nodes, operating at a telecommunication wavelength where the loss is lowest (Lines, 1984), such that the probability of transmitting a photon decreases exponentially with distance by only 0.2 dB/km. Assuming that one can realize a source of single photons with unity efficiency and the highest imaginable repetition rate, say, 1 THz, the success rate will drop from 7 GHz after 100 km to once every 164 years after 1000 km. Such low rates hinder quantum secure communication and the extension of quantum networks to global distances.

Not only the success rate but also the quality of entangled states decreases exponentially when the distance or the number of entangled particles is increased. The reason for this is that all operations required to control qubits (both locally and remotely) suffer from decoherence and technical imperfections, which accumulate with an increasing number of qubits and operations. Thus, the realization of large-scale quantum networks will require suitable protocols that counteract the accumulation of such imperfections. Such protocols are often termed "quantum error correction"(Devitt, Munro, and Nemoto, 2013).

A first idea how the mentioned challenges can be overcome in order to scale quantum networks to global distances was developed in 1998 (Briegel *et al.*, 1998) in the seminal quantum repeater protocol, whose basic idea is explained in Fig. 1. The proposed scheme involves the following key elements: first, probabilistic but heralded remote entanglement used in a repeat-until-success strategy; second, network nodes equipped with several multiplexed qubits, which can be individually controlled and coupled by deterministic operations; and third, a layer of quantum error correction, originally in the form of nested entanglement distillation (Bennett *et al.*, 1996).

The requirement of two-way signaling in the original scheme can be overcome using quantum error correction (Devitt, Munro, and Nemoto, 2013) instead of entanglement distillation. Even protocols without long-lived quantum memories can then be envisioned (Munro *et al.*, 2012), which may facilitate improved rates in certain parameter regimes but requires high-quality operations and low optical loss (Muralidharan *et al.*, 2016). In contrast, variants of the original scheme can be realized with experimental parameters that are accessible in the near term (Rozpedek *et al.*, 2018). Still, achieving the required multiplexing capacity and satisfying the high demands on efficiency and fidelity of all operations is a formidable experimental challenge. In this Colloquium, I first explain why the integration of qubits into optical resonators opens promising perspectives to this end. I then summarize the state of the art in cavity-enhanced quantum network nodes in the most promising experimental platforms studied thus far. Finally, I provide an outlook on the future prospects and challenges of these systems.

II. CAVITY-ENHANCED QUANTUM NETWORK NODES

The experimental realization of quantum networks requires stationary nodes with qubits that can be initialized, manipulated, entangled, and read individually with high fidelity. As shown in Fig. 1, this allows for the implementation of repeater architectures (Briegel *et al.*, 1998), in which the nodes hold two types of qubits: the first involves memory qubits that can store quantum states much longer than the time it takes to distribute entanglement over the network. To achieve this, the memory qubits should be decoupled from the optical channel but exhibit a deterministic and controlled coupling mechanism to the second qubit type, which is called communication qubits. The main purpose of these qubits is in turn to provide

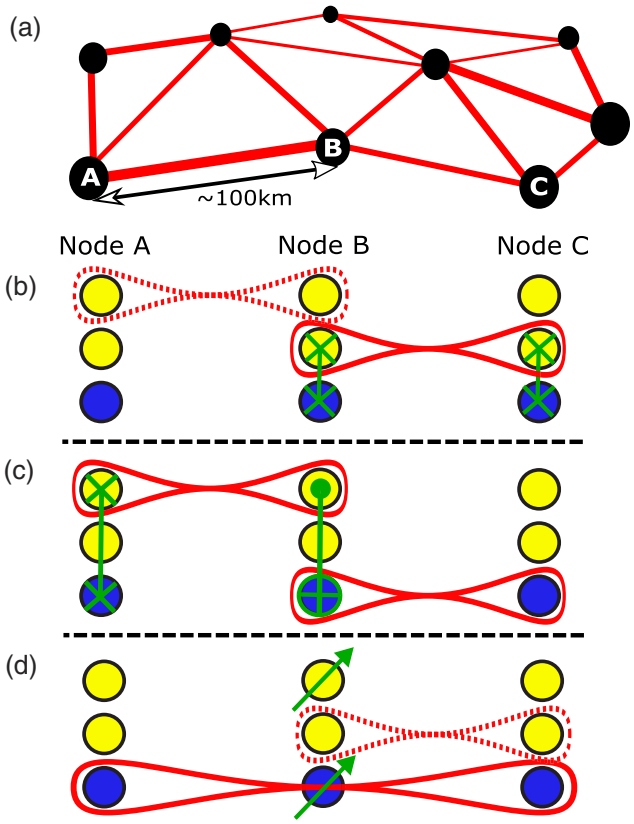

FIG. 1. Quantum network and quantum repeater scheme. (a) In a quantum network, qubits at stationary nodes (black) are connected by photons that travel along optical channels [red (gray)]. Photon loss limits the distance of direct links to ~100 km. (b) This limit can be overcome in a network architecture with memory and communication qubits. To this end, each node is equipped with several qubits (filled circles). A subset, called "communication" qubits (top row), couples to the optical channels for probabilistic entanglement generation (dashed symbol) between remote nodes. A herald unambiguously indicates when an entanglement attempt was successful (solid symbol). In this case, local two-qubit operations are used to swap the state of the communication qubits with the "memory" qubits (bottom row), which are isolated from the optical channels. (c) When memory qubits in neighboring segments have been entangled using a repeat-until-success strategy, local deterministic operations at the intermediate node can generate a maximally entangled cluster state of many qubits across the network. (d) A suited measurement of the inner qubits (arrows) can remove them from the cluster, generating an entangled state of memory qubits at the outer nodes even if their separation is too large for a direct photonic connection. Arbitrarily increasing the number or distance of entangled qubits is hampered by the loss of fidelity, which is exponential in the number of imperfect operations. To overcome this, new entanglement can be generated using the communication qubits (dashed), which may be then used to implement an error-correction layer, e.g., in the form of entanglement distillation (not shown).

an efficient and coherent interface to optical photons. Natural candidates for the communication qubits are single emitters, such as trapped ions (Duan and Monroe, 2010), neutral atoms (Reiserer and Rempe, 2015), quantum dots (Gao *et al.*, 2015; Lodahl, Mahmoodian, and Stobbe, 2015), molecules (Wang *et al.*, 2019), and spin qubits in solid-state host materials (Atatüre *et al.*, 2018; Awschalom *et al.*, 2018; Zhong and Goldner, 2019; Wolfowicz *et al.*, 2021). Often modeled as two-level systems, such emitters naturally exhibit nonlinear couplings (Chang, Vuletić, and Lukin, 2014). This allows for deterministic two-qubit quantum gates within the nodes, which can be an advantage compared to quantum networking protocols that only use quantum memories and linear optics, which are discussed in Sec. II.E.3.

The intrinsic nonlinearity of single emitters comes at the price of a moderate coupling to the photonic channels. Consider a single two-level atom that interacts with a resonant single-photon light pulse in free space (Leuchs and Sondermann, 2013). To achieve the best coupling, the light field would be focused to a diffraction-limited spot of the order of $A = (\lambda/2)^2$, with λ denoting the optical wavelength. To estimate the interaction probability, one has to compare this to the following absorption cross section of the emitter: $\sigma_{\mathrm{abs}} = 3\lambda^2/2\pi$. Albeit $A \simeq \sigma_{\mathrm{abs}}$ in this idealized situation, the photon absorption or scattering probability is in practice limited to about 20% due to finite solid angle coverage and imperfect spatial, temporal, and polarization mode matching (Leuchs and Sondermann, 2013). Coupling to several levels, which is present and strong in most emitters under study, leads to a further reduction. Therefore, better confinement of the electromagnetic field of the photon in both space and time is desirable for efficient quantum network nodes. This can be achieved by tailored nanophotonic waveguides (Vetsch *et al.*, 2010; Lodahl, Mahmoodian, and Stobbe, 2015) or by embedding the emitter into an optical resonator, which is the focus of this Colloquium.

In such a scenario, the physics of the coupled system is described by the Jaynes-Cummings Hamiltonian (Jaynes and Cummings, 1963), as detailed in the literature (Haroche and Raimond, 2013). The relevant figure of merit for the light-matter interaction and its dynamics is the cooperativity $C = g^2/2\kappa\gamma$, which is determined by three quantities: The first is the coupling constant g. The second is the polarization decay rate of the emitter $\gamma = \gamma_0 + \gamma_1 + \gamma_d$, which stems from its spontaneous decay on the cavity-coupled optical transition (at rate $2\gamma_0$) or other transitions ($2\gamma_1$), as well as its dephasing rate γ_d. Finally, the cavity field decay rate κ, which is the sum of the decay into free space κ_{loss} and into a desired output mode κ_{out}, as shown schematically in Fig. 2. Note that others (Janitz, Bhaskar, and Childress, 2020) have defined the energy rather than the field decay rates, which gives a factor of 2 in all equations.

Often, one further distinguishes between two regimes: that of "strong coupling," where $g \gg \kappa, \gamma$ and coherent reabsorption of photons is possible, and the "fast-cavity" regime with $\kappa > g \gg \gamma$ and $C \gg 1$. In both regimes, one gains access to efficient or even deterministic qubit-photon interactions (Borregaard, Sørensen, and Lodahl, 2019), an invaluable resource for quantum networking (Reiserer and Rempe, 2015) and repeaters of the first generation (Briegel *et al.*, 1998), and an indispensable prerequisite for high-rate quantum networks based on one-way quantum repeaters (Muralidharan *et al.*, 2016). The main advantages provided by optical resonators are described in

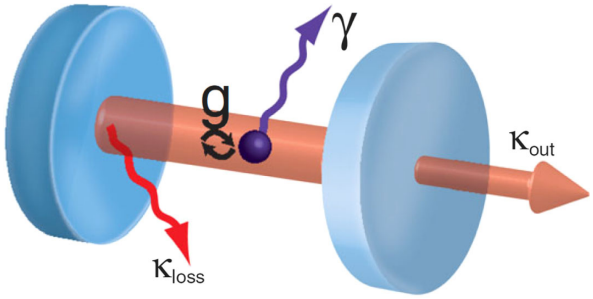

FIG. 2. Single emitter in an optical resonator. The electromagnetic field of a photon is tightly confined by two mirrors. A single emitter is located at the field maximum. The relevant rates are the emitter-cavity coupling (g), the decay of the emitter by spontaneous emission (at rate 2γ), and the field decay of the cavity both into free-space or absorbed modes (κ_{loss}) and into a desired output mode (κ_{out}).

Secs. II.A–II.E: enhanced photon generation and absorption, improved spin-state initialization and readout, and spin-photon quantum gates.

A. Spin-photon entanglement generation

In many protocols, the first step in entangling remote quantum network nodes is to entangle the spin of the communication qubits with single photons or photonic cluster states that are then sent along the optical channel (Reiserer and Rempe, 2015; Borregaard, Sørensen, and Lodahl, 2019). In free space, photon generation is typically realized by exciting the communication qubits with a short laser pulse, which is followed by spontaneous emission. If the emitter can decay via two transitions, the polarization of the photons can be entangled with the ground-state spin level (Blinov *et al.*, 2004), as shown in Fig. 3(b). Alternatively, for emitters with only a single transition, entanglement with the emission time bin is achieved using a suited sequence of ground-state spin manipulations (Barrett and Kok, 2005; Bernien *et al.*, 2013); see Fig. 3(c). In both settings, the obtained fidelity often depends on the excitation pulse duration, as the emitter can already decay during the pulse (Fischer *et al.*, 2017), thus projecting the state or leaving the intended initial state. While this limitation is reduced with short pulses, their use is often impeded by the requirement to not drive unwanted transitions to other excited state levels.

As in the free-space scenario, photon generation by excitation with a short resonant laser pulse can also be implemented when the emitter is placed in a resonator; see Fig. 3(a). If the emitter dephasing is not the dominant rate, which is the typical situation in quantum networking experiments, the dynamics of the decay will be strongly modified. As the density of photonic modes is changed by the resonator, one can obtain the followed increased (Purcell, 1946) or decreased (Kleppner, 1981) radiative decay rate (Haroche and Raimond, 2013):

$$\gamma_c = \frac{g^2\kappa}{\kappa^2 + \Delta^2}. \tag{1}$$

As one can see, the decay into the resonator γ_c is suppressed when Δ, the detuning between emitter and cavity mode, is increased. On resonance, one finds that the decay rate is enhanced by the Purcell effect (Purcell, 1946) $\gamma_c = P\gamma_0$, where the Purcell factor P is related to the cooperativity via

$$P = 2C\frac{\gamma}{\gamma_0}. \tag{2}$$

In the limit of a large Purcell factor $\gamma_c \gg \gamma_0 + \gamma_1$, such that the radiative decay of the emitter into the resonator is much faster than its decay into free-space modes. This has several beneficial effects in the context of quantum networks: First, when the resonator is overcoupled, i.e., the cavity field decay κ is dominated by the coupling into a single propagating mode κ_{out}, one can strongly improve the photon collection probability and thus the efficiency of spin-photon entanglement generation. Second, one can enhance the photon generation rate, which is particularly relevant for emitters with slow radiative decay. But also for emitters that exhibit fast

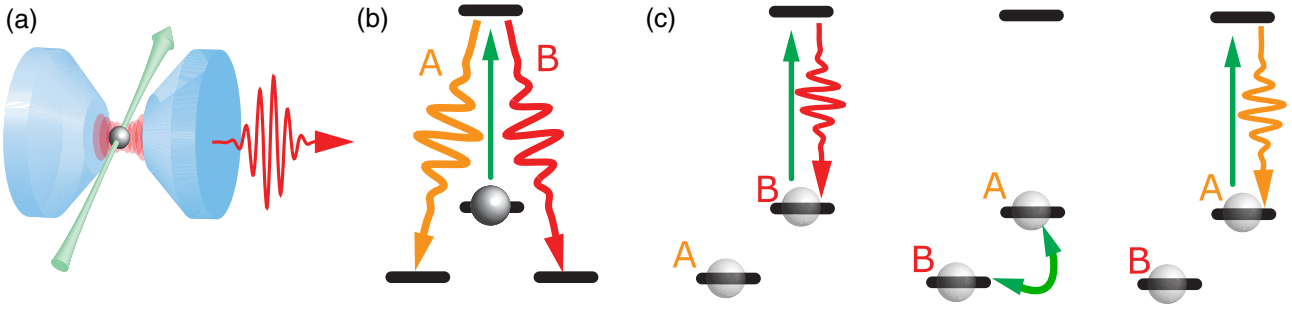

FIG. 3. Generation of spin-photon entanglement. (a) Single emitter excited with a laser pulse (arrow). It decays back to the ground state while emitting a single photon (curly arrow), which is efficiently collected by the resonator. (b) Level scheme with two optical transitions. After optical excitation (straight arrow), the emitter can decay to two different levels (A and B) by emitting light at different polarization or frequency. If the transitions have equal probability and are both supported by the cavity, a maximally entangled Bell state is generated. (c) Protocol with a single optical transition. The qubit is prepared in a superposition between the two ground states (A and B). In a first step (left), the emitter is excited and emits a photon only if it is in state B. After swapping the ground-state populations, a second pulse excites the spin only if it is in A. For a balanced superposition, the scheme generates entanglement between the spin state and the emission time bin of a photonic qubit.

dephasing or considerable spectral diffusion, the increased decay rate can dramatically improve the coherence and spectral purity that is required for remote entanglement. Third, an advantage of the resonator is that it may enhance the emission into one out of several optical transitions, such as into a desired atomic ground state (see Sec. III.B.1) or crystal field level (Liu and Jacquier, 2005) (see Sec. III.B.3). Similarly, some emitters (see Sec. III.B.2) exhibit an undesired coemission of phonons whose contribution can be suppressed by the cavity-enhanced decay. Finally, the presence of a resonator enables efficient photon generation and photon absorption via off-resonant Raman transitions, which is detailed in the following.

B. Stimulated Raman transitions

The aforementioned scheme of photon generation by fast resonant excitation of a two-level system is applicable to any quantum emitter but has intrinsic limitations to the spin-photon entanglement fidelity caused by the mentioned emission during the pulse (Fischer *et al.*, 2017). In addition, the laser pulse has to be well separated from the single-photon pulses by spatial (Bochmann *et al.*, 2008), temporal, or polarization filtering (Bernien *et al.*, 2013). To improve the fidelity, one can use emitters with another ground-state level in a lambda configuration (Wilk *et al.*, 2010). Here scattered pump light can be filtered spectrally (Sipahigil *et al.*, 2016), and the photon emission frequency can be widely tuned (Mücke *et al.*, 2013; Sipahigil *et al.*, 2016). In addition, reexcitation of the emitter is avoided when the ground-state level spacing is sufficient, enabling spin-photon entanglement with high fidelity ($\gtrsim$99% at $\sim$30% success probability) (Ritter *et al.*, 2012), even beyond typical error-correction fidelity thresholds in topological quantum computing (Fowler *et al.*, 2012; Nickerson, Li, and Benjamin, 2013).

When the emitter is placed in a cavity, spectral filtering is intrinsically implemented by the resonator. Even more important, photon generation is made efficient and reversible (Cirac *et al.*, 1997) when one uses a scheme called vacuum-stimulated Raman adiabatic passage, pioneered with trapped atoms (Kuhn *et al.*, 1999) and later adapted to cavity-coupled solid-state emitters (Sun *et al.*, 2018). The scheme can be implemented in both the Purcell and the strong-coupling regime. To this end, the intensity of an external control laser is varied only on a slow timescale, such that the system is kept in a coherent Raman dark state. When the control is ramped up, exactly one photon is emitted from the resonator. The electromagnetic field mode of the photon is determined by the properties of the control laser pulse (Morin *et al.*, 2019). Similarly, when the control field is ramped down, an impinging photon with a matching temporal mode is absorbed (Boozer *et al.*, 2007), and its polarization can be mapped to the spin state of the emitter (Specht *et al.*, 2011), as shown in Fig. 4. This can be used to realize an efficient protocol for remote entanglement (Ritter *et al.*, 2012). As the original atomic state is depleted, the scheme can be combined with state detection (detailed later) to herald successful entanglement attempts over a lossy channel.

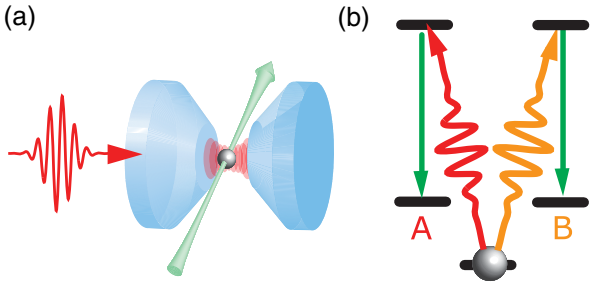

FIG. 4. Photon absorption using a stimulated Raman transition. (a) Impinging photon (curly arrow) transferred to the spin of a single emitter in a cavity using a Raman laser beam (straight arrow). (b) Level scheme. Depending on the qubit encoded in the photon, such as in its polarization or frequency, the emitter is transferred to a different internal state (A or B).

C. Spin initialization and readout

A key capacity for the processing of quantum information is the ability to perform a faithful projective measurement of the qubit state. Ideally, this readout procedure is robust and fast enough to allow for feedback onto the quantum state, which is a prerequisite for measurement-based quantum information processing (Briegel *et al.*, 2009), entanglement distillation (Bennett *et al.*, 1996; Kalb *et al.*, 2017), and quantum error correction in the network (Nickerson, Li, and Benjamin, 2013).

With emitters in free space, the quantum state is typically measured via photon scattering on a closed transition (Leibfried *et al.*, 2003). High readout fidelity is achieved when at least one scattered photon is detected before the spin decays to other levels via unwanted optical transitions or other decay mechanisms. First, this requires frequency-selective excitation of only one qubit state; second, a fast cycling transition that decays predominantly back to the original state; and, third, highly efficient detectors and collection optics. Each of the aforementioned criteria is improved when the emitter is placed in an overcoupled optical resonator that enhances the emission into a propagating light mode (Bochmann *et al.*, 2010). When $P \gg 1$, single-shot readout can be achieved even with emitters that lack a closed transition (Kindem *et al.*, 2020; Raha *et al.*, 2020).

However, the resonator also facilitates a different detection method, as the cavity transmission and reflection properties are altered by the presence of an emitter in a coupled energy level (Boozer *et al.*, 2007). If the emitter and resonator frequency are known and stable and in a regime where $C \gg 1$, this allows for state detection without photon scattering (Volz *et al.*, 2011), which again means that the procedure works reliably for emitters that lack a closed transition.

The described techniques leave the qubit in the measured quantum state, such that they can also be used for state initialization. However, optical pumping is often used to this end. Here the idea is to repeatedly excite the emitter until it has decayed to the desired state, which should be the only level that is not pumped. The fidelity of the process depends on the ratio of the desired pumping rate versus that of off-resonant driving on unwanted transitions, and on the lifetime of the

ground state. Again, a resonator can enhance this process by improving the frequency selectivity and speeding up the decay rate. Combining optical pumping with subsequent state detection may then provide an optimal initialization procedure in terms of speed and fidelity (Reiserer, Ritter, and Rempe, 2013).

D. Spin-photon quantum gates

Sections II.A–II.C described the generation and absorption of photons from a cavity-coupled emitter. But the resonator also enables another, deterministic interaction mechanism of coupled stationary qubits with impinging photons that are reflected from it (Hofmann *et al.*, 2003; Duan and Kimble, 2004; Borregaard, Sørensen, and Lodahl, 2019). In particular, when $C \gg 1$, a spin-photon quantum gate can be realized without photon absorption or scattering. For an intuitive explanation of the mechanism, consider an emitter in a lossless, overcoupled cavity in the strong-coupling regime, see Fig. 5(a). A resonant photon is reflected off the coupling mirror, which has a small transmission. If there is no emitter in the resonator or the emitter is in an uncoupled qubit state, the light field leaking out of the resonator interferes destructively with the direct reflection at the coupling mirror, which means that the photon experiences a phase shift of π. If, however, a resonant emitter is present, the energy eigenstates of the coupled system are split (Reiserer and Rempe, 2015). Thus, an impinging photon will now be off resonant, meaning that it cannot enter the resonator but is reflected off the coupling mirror without a phase shift.

In effect, the reflection process leads to a conditional phase shift of π between the emitter and the photon, i.e., a controlled-phase quantum gate. After first experiments with trapped atoms (Reiserer, Ritter, and Rempe, 2013; Reiserer *et al.*, 2014; Tiecke *et al.*, 2014; Volz *et al.*, 2014), quantum gates based on this mechanism have also been realized with superconducting qubits (Kono *et al.*, 2018), quantum dots (Sun *et al.*, 2018), and spins in diamond (Nguyen *et al.*, 2019). The fidelity of the scheme is robust to many experimental imperfections as long as the spatial mode and frequency of the photons match that of the emitter-cavity system. In particular, the magnitude of the phase shift does not depend on the precise emitter-cavity coupling strength and detuning, making the scheme well suited for emitters with considerable spectral diffusion. The bandwidth of faithful operation is determined by the slope of the curves in Fig. 5: in the strong-coupling regime, it is set by the cavity decay κ, whereas in the Purcell regime it depends on the enhanced emitter decay rate g^2/κ (Kalb *et al.*, 2015).

For an ideal system, the previously explained scheme is deterministic. In practice, the efficiency and fidelity can be reduced by imperfect optical mode matching, by cavity scattering loss, and by a finite cooperativity. The scaling with finite cooperativity was the subject of several theoretical works that investigated entanglement generation or quantum gates based on cavity-induced phase shifts. Depending on the protocol used, one finds a scaling of the failure probability $\propto 1/\sqrt{C}$ (Sørensen and Mølmer, 2003) or $\propto 1/C$ (Kastoryano, Reiter, and Sørensen, 2011). Again, using the concept of heralding, one can achieve almost perfect fidelity as long as $C > 1$, at the price of a success rate reduction that depends on C (Borregaard *et al.*, 2015; Borregaard, Sørensen, and Lodahl, 2019).

The first experiment that implemented the previous gate mechanism with trapped atoms at $C \simeq 3$ generated entangled states with 81% fidelity (Reiserer *et al.*, 2014), limited mainly

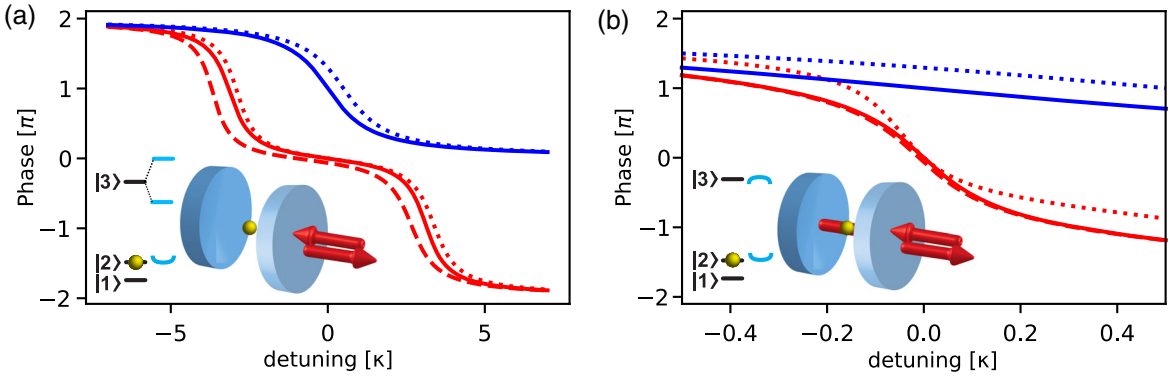

FIG. 5. Cavity-based quantum gates. The calculated phase difference as a function of the photon detuning (in units of the cavity linewidth κ) for systems with $C = 50$ in (a) the strong-coupling regime ($g = \sqrt{10}\kappa > \kappa > \gamma = \kappa/10$) and (b) the Purcell regime ($\kappa > g = \kappa/\sqrt{10} > \gamma = \kappa/1000$). On resonance, a coupled emitter [red (gray) lines] leads to a phase shift of π with respect to the case of an empty cavity or an uncoupled emitter [blue (dark gray) lines], almost independent of the emitter detuning ($\Delta_e = 5\gamma$; dashed line), but sensitive to the cavity detuning ($\Delta_c = 0.5\kappa$; dotted line). Insets: Phase-shift mechanism. A single photon (arrows) is reflected from a single-sided optical resonator that contains a single emitter. The transition between the emitter energy levels (left) $|2\rangle$ and $|3\rangle$ is on resonance with the cavity frequency. When the emitter is in an off-resonant state $|1\rangle$, the light field enters the resonator before it is reflected, acquiring a phase shift of π. In the resonant emitter state $|2\rangle$; however, there is no phase shift of the combined emitter-photon state. (a) In the strong-coupling regime the energy spectrum is split (dashed lines). Thus, the photon is reflected without entering the resonator, acquiring no phase shift. (b) In the Purcell regime, the light field enters the cavity. It drives the emitter to the excited state from which it decays back into the cavity mode. In this process, both the emitter and the photon acquire a π phase shift such that their difference is again zero.

by imperfect optical mode matching and single-qubit control. The current record was achieved with the Si-V center in diamond with $C \simeq 10^2$ and an entangled-state fidelity of 94%. While this number is encouraging for the implementation of quantum repeaters of the first generation (Briegel *et al.*, 1998; Muralidharan *et al.*, 2016), further improvements will be necessary for implementing one-way quantum repeaters that require much higher fidelity operations, for instance, 99.9% was found by Borregaard *et al.* (2020). Still, such schemes may eventually become feasible using cavity-coupled emitters with deterministic spin-photon coupling (Borregaard, Sørensen, and Lodahl, 2019).

E. Remote entanglement protocols

As summarized in Secs. II.A–II.D, optical resonators can be used to enhance the capabilities of quantum network nodes. In the following, I describe the application of these techniques toward the generation of heralded entanglement between remote communication qubits, which is a key resource for quantum networks and required for first-generation quantum repeaters (Briegel *et al.*, 1998; Muralidharan *et al.*, 2016). In this context, two major approaches can be discriminated: first, entanglement swapping by photonic Bell-state measurements and, second, entanglement transfer by heralded absorption, as sketched in Fig. 6.

1. Entanglement swapping

In the first approach, both quantum network nodes generate spin-photon entanglement using the techniques described in Secs. II.A and II.B. The two photons are then sent to a photonic Bell-state analyzer, which is typically realized by linear optical elements and single-photon detectors. Coincidence detection events then allow one to distinguish two out of four photonic Bell states (Calsamiglia and Lütkenhaus, 2001), which is sufficient for heralded remote entanglement via entanglement swapping (Żukowski *et al.*, 1993). In principle, the intrinsic inefficiency can be avoided by photonic quantum gates that use deterministic schemes (Hacker *et al.*, 2016; Stolz *et al.*, 2022), but thus far have not reached the robustness, simplicity, or efficiency of linear optical setups.

The physical effect that enables the Bell-state measurement in linear optical setups is two-photon quantum interference (Hong, Ou, and Mandel, 1987). Note, however, that single-photon interference protocols have also been proposed (Cabrillo *et al.*, 1999) that may offer increased rates in a high-loss regime (Campbell and Benjamin, 2008), as successfully demonstrated by Kalb *et al.* (2017). In all such protocols, the mechanism works only if the photons are indistinguishable in all degrees of freedom except the one that encodes the entanglement with the spin (Reiserer and Rempe, 2015). This enforces accurate control over the photon emission time, frequency, polarization, and wave packet, which is difficult to achieve in practice, leading to a reduction in fidelity. Still, the fidelity may be improved at the price of a reduced success probability when the interference signal is recorded with high temporal resolution and when only events that occur within a short arrival time difference are considered (Bernien *et al.*, 2013; Nölleke *et al.*, 2013). The aforementioned approach also works in the absence of a cavity (Moehring *et al.*, 2007; Bernien *et al.*, 2013), and reasonable efficiencies can be achieved in systems with strong optical transitions and

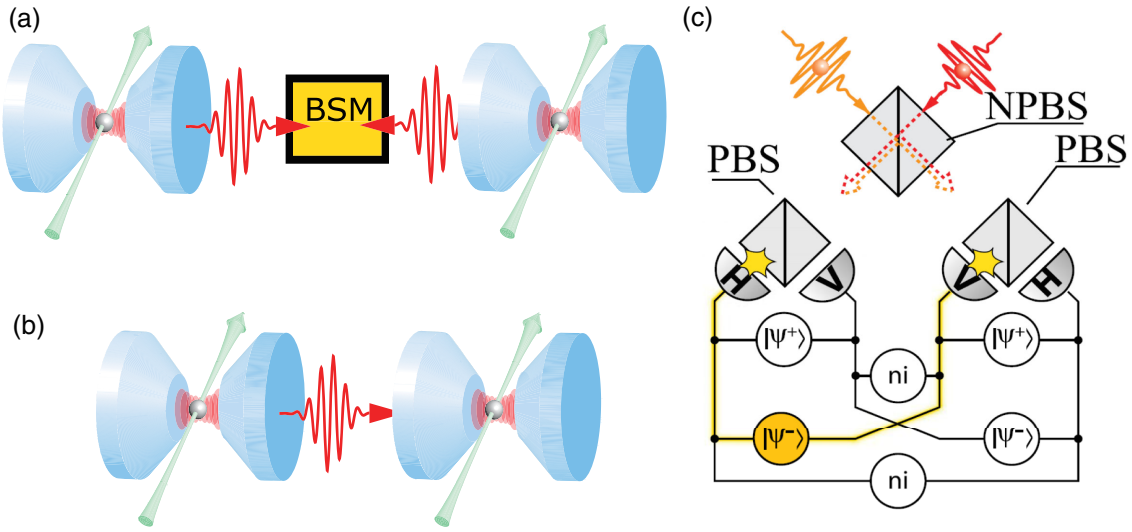

FIG. 6. Protocols to generate remote entanglement. (a) Entanglement swapping. An entangled spin-photon state is first generated at both quantum network nodes. The photons impinge on a setup that allows for a measurement of the photonic Bell state (BSM). (b) Entanglement by heralded absorption. Spin-photon entanglement is generated at the left node. The photon is sent to the second node, where it is absorbed such that the encoded quantum state is transferred to the spin of the emitter. (c) Linear optical Bell-state measurement for polarization qubits. The photons impinge on a nonpolarizing beam splitter (NPBS), followed by two polarizing beam splitters (PBSs) with single-photon detectors in their horizontal (H) and vertical (V) output ports. A coincidence detection in two of the output ports heralds a specific Bell state $|\Psi^+\rangle$ or $|\Psi^-\rangle$, depending on which detectors fire (yellow). In the other Bell states, photons have the same polarization and will thus leave the NPBS in the same output port. Therefore, coincidences with the same polarization indicate that the other photon properties were not identical (ni).

optimized collection (Stephenson *et al.*, 2020). Embedding the emitter into a resonator can improve the rate and fidelity by enhancing the photon emission and collection probability, as detailed in Sec. II.A.

2. Heralded absorption

A second approach to remote entanglement generation that is enabled or enhanced by optical resonators uses heralded photon absorption, which overcomes the efficiency limitation of photonic Bell-state analyzers (Lütkenhaus, Calsamiglia, and Suominen, 1999) and can be more robust with respect to experimental imperfections. The process starts with spin-photon entanglement at one node. At the other node, the state of the photonic qubit is then transferred to the spin, as shown in Fig. 6(b). To allow for repeat-until-success entanglement, successful transfer has to be heralded.

There are two options for achieving this task: In the first option, the absorption process is the time reversal of the photon emission, in which a stimulated Raman adiabatic passage is used (Cirac *et al.*, 1997) with multilevel emitters. This protocol can achieve the highest success probability and fidelity reported to date (Ritter *et al.*, 2012). To herald successful qubit transfer, one has to detect whether or not the emitter has remained in its initial state, which can be accomplished using the techniques described in Sec. II.C. Alternatively, the control laser field can be replaced by the vacuum field of a second resonator. The detection of a scattered Raman photon then signals qubit transfer to the spin (Brekenfeld *et al.*, 2020).

The second option for heralded photon storage is based on the cavity-based spin-photon quantum gate mechanism described in Sec. II.D. The first realization used a gate operation with a combination of spin manipulations, photon detection, and active feedback (Kalb *et al.*, 2015). Recently this approach has been used to generate entangled states by implementing a quantum gate between remote emitters (Daiss *et al.*, 2021), highlighting its potential for quantum networks.

3. Ensemble-based approaches

Thus far we have focused on single emitters as quantum network nodes. This has the advantage that the nonlinearity of the emitters allows for deterministic qubit interactions within a node, which improves the efficiency of first-generation repeaters and enables second- and third-generation quantum repeaters (Muralidharan *et al.*, 2016). However, using single emitters requires resonators of high quality. This difficulty is avoided when one uses the collective enhancement of the light-matter interaction with ensembles of emitters (Hammerer, Sørensen, and Polzik, 2010). In addition, in this approach the exponential loss in optical fibers can be overcome with suited quantum repeater schemes, the first of which is often called the Duan-Lukin-Cirac-Zoller (DLCZ) protocol (Duan *et al.*, 2001). In this scheme, atomic ensembles serve as both photon sources and quantum memories. Entanglement between remote ensembles is achieved in a repeat-until-success strategy by interfering emitted photons on a beam splitter. This induces a measurement-based nonlinearity, similar to that in related concepts for photonic quantum computing (Knill, Laflamme, and Milburn, 2001).

The main protocols and first experimental implementations of quantum networking with atomic ensembles were summarized by Sangouard *et al.* (2011). Early milestone experiments include the probabilistic entanglement (Chou *et al.*, 2005) of up to four different ensembles (Choi *et al.*, 2010) using atoms in vacuum. Later ensembles in solid-state platforms were employed to realize DLCZ-type photon sources (Kutluer, Mazzera, and de Riedmatten, 2017; Laplane *et al.*, 2017), and the scheme has even been applied to entangle vibrations of remote optomechanical resonators (Riedinger *et al.*, 2018).

While the original DLCZ scheme used ensembles as both quantum memory and entanglement source, the latter can also be implemented using other techniques, such as nonlinear optics. As an example, sources based on spontaneous parametric downconversion (SPDC) (Zhang *et al.*, 2021) can facilitate a speedup of the remote entanglement rate when they are combined with efficient and broadband quantum memories (Simon, de Riedmatten *et al.*, 2007). Such devices can be realized with ensembles of trapped atoms or dopants in certain host crystals (Lvovsky, Sanders, and Tittel, 2009; Tittel *et al.*, 2010; Afzelius, Gisin, and de Riedmatten, 2015), offering a large multiplexing capacity (Usmani *et al.*, 2010; Afzelius, Gisin, and de Riedmatten, 2015; Seri *et al.*, 2017) that can be utilized in tailored quantum repeater protocols (Sinclair *et al.*, 2014) to facilitate high-rate remote entanglement. The first experiments along these lines were the storage of entangled photons in two crystals (Clausen *et al.*, 2011; Saglamyurek *et al.*, 2011), also heralded after interfering photons at telecommunications wavelength (Lago-Rivera *et al.*, 2021). Other recent advances include the combination of an atomic ensemble photon source with a crystal-based memory (Maring *et al.*, 2017) and the entanglement of trapped-atom ensembles over 50 km of fiber (Yu *et al.*, 2020). The latter experiments used frequency conversion to the telecommunications frequency band, a prerequisite for entanglement over many kilometers of optical fibers.

While the previously cited studies were performed without optical resonators, their use can enhance the efficiency of both photon storage and photon generation. When one uses a SPDC source, cavities can reduce the required optical driving power, give higher source brightness, improve the mode matching to single-mode fiber, and facilitate spectral filtering, as summarized by Slattery *et al.* (2019). When emitter ensembles are used as the photon source, their integration into optical resonators can lead to a high brightness (Thompson *et al.*, 2006) and enable a high readout efficiency of a stored excitation (Simon, Tanji, Thompson, and Vuletić, 2007). Furthermore, cavities can enhance other entanglement generation protocols, such as rephased amplified spontaneous emission (Williamson and Longdell, 2014).

Regarding the storage of photons, cavities can boost the efficiency. The achievable enhancement can be understood semiclassically (Tanji-Suzuki *et al.*, 2011) or treated in a quantum-mechanical framework (Gorshkov *et al.*, 2007; Afzelius and Simon, 2010). Typical experiments use atoms in vacuum (Tanji *et al.*, 2009) or rare-earth-doped crystals (Sabooni *et al.*, 2013; Jobez *et al.*, 2014). The enhancement of the light-matter-interaction strength offered by a cavity facilitates efficient quantum memories with a compact footprint, even down to nanophotonic devices (Zhong *et al.*, 2017;

Wallucks *et al.*, 2020). Furthermore, the use of optical resonators can suppress the noise in multiplexed quantum memories (Heller *et al.*, 2020), enable couplings between different memory modes (Simon, Tanji, Ghosh, and Vuletić, 2007), and realize additional functions such as light-pulse switching by stored photons (Chen *et al.*, 2013) if $C > 1$.

A drawback of the previously presented ensemble-based schemes is the absence of an intrinsic nonlinearity. Thus, in both the DLCZ- and SPDC-based approaches the photon sources have to operate at a low efficiency to avoid the simultaneous emission of uncorrelated photons. Experimental imperfections lead to a further reduction of the remote entanglement rate, thus hampering large-scale quantum networks. To overcome this difficulty, adding a nonlinear processing capacity to resonator-enhanced ensembles seems to be attractive. The main approaches are based on the Coulomb interaction between trapped ions (Lamata *et al.*, 2011; Casabone *et al.*, 2015) and on Rydberg interactions in ensembles of neutral atoms. The latter facilitate interactions between photons (Firstenberg *et al.*, 2013), and even photon-photon quantum gates in a free-space setting (Tiarks *et al.*, 2019). The use of optical resonators can dramatically enhance the efficiency of such approaches, with a recent experiment demonstrating $> 40\%$ efficiency (Stolz *et al.*, 2022).

III. EXPERIMENTAL REALIZATIONS

A. Optical resonator designs

Thus far we have focused on the underlying concepts of cavity-enhanced quantum network nodes. In the following, the current state of the art of experimental systems is summarized. An optical resonator that allows for the implementation of an efficient quantum interface to single emitters should fulfill the following two conditions: $\kappa_{\text{out}} \gg \kappa_{\text{loss}}$ and $C \gg 1$. This indicates the requirement for resonators with a small mode volume V and a large quality factor Q as $C \propto Q/V$ (Lodahl, Mahmoodian, and Stobbe, 2015; Reiserer and Rempe, 2015; Janitz, Bhaskar, and Childress, 2020). There are several approaches to realizing such a resonator (Vahala, 2003), the most prominent being Fabry-Perot, ring, and photonic-crystal resonators, as shown in Fig. 7.

Fabry-Perot resonators consist of two curved mirrors at a short distance, as shown in Fig. 7(a). To achieve high quality factors, one uses Bragg reflectors, which consist of dielectric layers with alternating refractive indices, often Ta_2O_5 and SiO_2 with $n \simeq 2.1$ and 1.4, respectively. The reflectors have to be deposited on atomically flat substrates to avoid excess loss by scattering. Transmission and scattering losses both below 1 ppm per mirror can be achieved with commercially available superpolished mirrors (Rempe *et al.*, 1992), which leads to a finesse of around $\mathcal{F} = 2 \times 10^6$, and even higher $Q = n\mathcal{F}$, where the mode number n counts the half waves in the resonant cavity. In typical experiments, cooperativities of around 10 are achieved using this approach (Reiserer and Rempe, 2015). Alternatively, low-roughness depressions with smaller radius of curvature can be fabricated by etching (Wachter *et al.*, 2019) or laser machining (Hunger *et al.*, 2012), both of which enable finesse values beyond 2×10^5 and small mode volumes approaching a single cubic wavelength (Najer *et al.*, 2019).

Emitters can be integrated into the resonator either by trapping atoms in vacuum (Reiserer and Rempe, 2015) or by depositing a nanocrystal (Kaupp *et al.*, 2016; Casabone *et al.*, 2018) or a thin crystalline membrane (Janitz *et al.*, 2015; Bogdanovic *et al.*, 2017; Riedel *et al.*, 2017; Merkel,

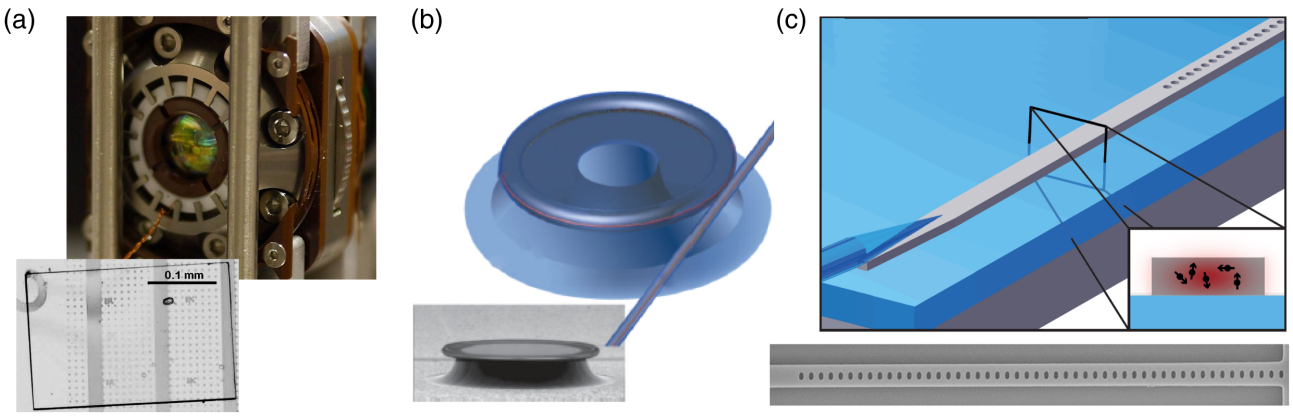

FIG. 7. Types of optical resonators. (a) Top image: experimental realization of a cryogenic Fabry-Perot cavity. The separation (< 0.1 mm) of the two mirrors at the center is controlled using a piezoelectric tube (white ring) that presses against stiff titanium springs (gray), achieving length fluctuations $\lesssim 1$ pm. The setup is mounted using soft polymer springs (dark, side of the assembly) that isolate it from environmental vibrations. From Merkel, 2021. Bottom: microscopic image of a diamond membrane with dimensions $0.01 \times 0.3 \times 0.2$ mm^3 deposited on a Bragg reflector. Microwave striplines (dark gray) allow for the application of microwave pulses to emitters in the membrane. (b) Ring resonator in the form of a microtoroid that supports a whispering-gallery mode with a high quality factor. The coupling to a nearby nanofiber can be adjusted via their distance. Bottom image: scanning electron microscope image of a resonator with a diameter of 120 μm. Adapted from Vahala, 2003. (c) Photonic-crystal resonator. Top image: schematic of the setup. Using a conically tapered fiber, one couples photons to a nanophotonic waveguide feeding the resonator at its end. Individual emitters are integrated into the resonator material, as seen in its cross section (inset). From Weiss *et al.*, 2021. Bottom: scanning electron microscope image of a resonator, formed using a periodic arrangement of holes along a silicon waveguide with a separation of ~ 0.3 μm.

Ulanowski, and Reiserer, 2020; Ulanowski, Merkel, and Reiserer, 2022) on one of the mirrors. Experimentally achieved cooperativities (Colombe *et al.*, 2007) and Purcell factors (Merkel, Ulanowski, and Reiserer, 2020; Ulanowski, Merkel, and Reiserer, 2022) are of the order of 10^2. Coupling to the resonator mode is achieved by free-space optics (with $> 99\%$ efficiency) or by directly coupling to a single-mode fiber with $\sim 90\%$ efficiency (Gulati *et al.*, 2017; Niemietz *et al.*, 2021).

Compared to the other, later described approaches, Fabry-Perot resonators have two major advantages: First, they can be stabilized and tuned over many free spectral ranges using piezoelectric positioners. Second, to first order the Purcell factor does not depend on the cavity length L, as $Q \propto L$ and $V \propto L$. Thus, without reduction of the Purcell factor an emitter can be kept a large distance from all interfaces, which avoids the undesired influence of surface charges and paramagnetic trap states on the emitter stability.

A second approach to implement resonators with a large Purcell factor uses ring resonators, as shown in Fig. 7(b), either based on a whispering-gallery mode in microtoroids (Aoki *et al.*, 2006), microspheres (Shomroni *et al.*, 2014), or bottle resonators (Pöllinger *et al.*, 2009) or using nanophotonic waveguide ring or racetrack resonators (Bogaerts *et al.*, 2012). Emitters in the mode can exhibit a chiral coupling to light, leading to new possibilities for spin-photon interfaces (Lodahl *et al.*, 2017). Tuning is typically achieved by temperature (Aoki *et al.*, 2006) or, with bottle resonators, mechanically (Pöllinger *et al.*, 2009). Experimentally achieved cooperativities with atoms (Aoki *et al.*, 2006; Junge *et al.*, 2013; Scheucher *et al.*, 2016; Bechler *et al.*, 2018) and Purcell factors with defect centers (Faraon *et al.*, 2011) are of the order of 10, and high coupling efficiency is obtained via tapered fibers.

The third approach for efficient light-matter coupling is based on photonic-crystal resonators (Lodahl, Mahmoodian, and Stobbe, 2015; Asano and Noda, 2018), as shown in Fig. 7(c). When coupled to single emitters, cooperativities approaching 10^2 (Samutpraphoot *et al.*, 2020) and Purcell factors approaching 10^3 (Dibos *et al.*, 2018) have been reported. Optimized structures in silicon even enable $Q > 10^7$ (Asano *et al.*, 2017) at mode volumes of around λ^3. When one uses dielectric enhancement, the effective mode volume can be further reduced by 3 orders of magnitude (Hu *et al.*, 2018) while maintaining high Q. To use such a structure for quantum network nodes, however, the communication qubits have to be placed in the dielectric material of the resonator, which limits the applicability of the approach to specific combinations of emitter and host. Furthermore, the proximity of interfaces will likely degrade the coherence of the emitter in such a setting. Finally, care has to be taken in the evaluation of the cooperativity, as the dipole approximation assumes that the electric field changes only on a scale that is comparable to the wavelength (Cohen-Tannoudji, Dupont-Roc, and Grynberg, 1989), which is not satisfied in structures with deeply subwavelength dielectric features.

Tuning of photonic-crystal cavities has been demonstrated using many techniques, including gas condensation (in the case of cryogenic resonators) (Mosor *et al.*, 2005), nanomechanical actuation (Chew *et al.*, 2010), electro-optical shifting (Lu *et al.*, 2012), and temperature (Tiecke *et al.*, 2014). To couple into the resonators, different techniques can be used. The highest efficiencies (97%) are achieved using an adiabatic transition of the guided mode of a tapered optical fiber to that of a high-index dielectric waveguide (Tiecke *et al.*, 2015) feeding the cavity. Other approaches use cleaved or lensed fibers with mode converters at the chip edge or diffraction gratings at the chip center, with typical efficiencies of 50% (Vivien and Pavesi, 2013).

B. Experimental platforms

In this section, the physical systems that are used as communication qubits are described. As mentioned, their main purpose is to provide an efficient interface to photons, which is achieved using a suited optical resonator. Ideally, the photon wavelength will fall in the so-called telecommunications window, between 1500 and 1600 nm, where the loss of germanium-doped silica optical fibers is minimal (Lines, 1984), around 0.2 dB/km; see Fig. 8(a). While optical fiber links with lower loss would be desirable for global networks, no such system has been demonstrated, in spite of an intense search over several decades. Still, when using the existing infrastructure, photonic qubits can be transmitted over many kilometers with negligible decoherence even at room temperature and with moderate loss; see Fig. 8(b).

The most prominent physical systems explored thus far to couple to these photons are single atoms (green circles in Fig. 8), impurities in diamond, silicon, or silicon carbide (red circles), and rare-earth dopants (blue circles). Quantum dots with their wide tunability are not included in Fig. 8, as it seems difficult to combine them with memory qubits that offer sufficient coherence for long-distance networks (Lodahl, Mahmoodian, and Stobbe, 2015). Furthermore, the figure contains only those transitions that have been investigated in experiments, which all originate from a long-lived ground state. It has been proposed that transitions in the excited state manifold of neutral atoms may offer telecommunications (telecom) compatibility when resonators with large cooperativity are used (Uphoff *et al.*, 2016; Covey *et al.*, 2019; Menon *et al.*, 2020), but an experimental demonstration is still missing.

Figure 8(b) thus indicates that most investigated systems will require efficient transduction of the photon frequency (Zaske *et al.*, 2012) when large distances are targeted. This will add complexity and cost while reducing the efficiency and fidelity. Still, recent advances have enabled entanglement-preserving telecom conversion from visible emitters (De Greve *et al.*, 2012; Bock *et al.*, 2018; Tchebotareva *et al.*, 2019; van Leent *et al.*, 2020), thus demonstrating the feasibility of the approach.

As an alternative, emitters in the minimal loss band of optical fibers, i.e., between ~ 1250 and ~ 1650 nm, can be used. These include defect centers in silicon (Bergeron *et al.*, 2020; Durand *et al.*, 2021) and silicon carbide (J.-F. Wang *et al.*, 2020) (with currently unknown optical coherence), as well as erbium dopants. The optical transitions of erbium dopants can exhibit noteworthy coherence of several milliseconds in some host materials (Böttger *et al.*, 2006), approaching the lifetime limit in suited resonators (Merkel,

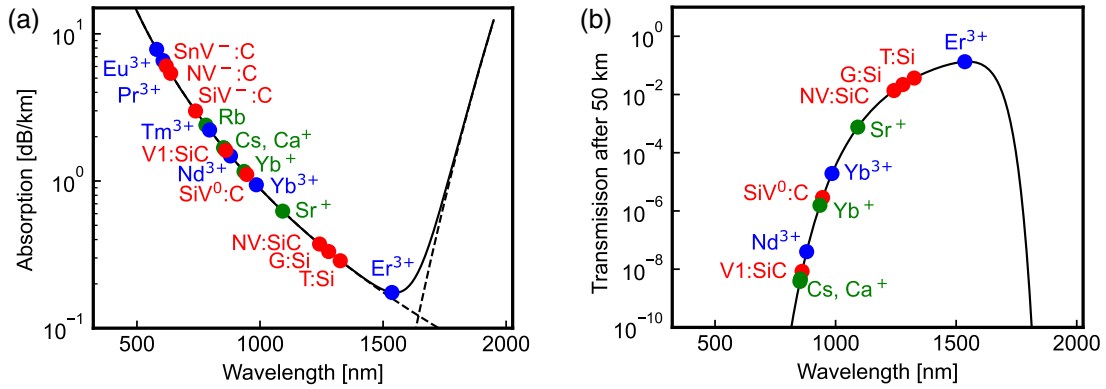

FIG. 8. Loss in optical fibers. (a) Absorption coefficient (black solid line) of ultrapure "dry" silica fiber caused by Rayleigh scattering and infrared absorption (black dashed lines). Only a few emitters [defects in diamond (C) and other semiconductors (Si and SiC), atoms in vacuum (Rb, Cs, Ca^+, and Yb^+); rare-earth dopants (Tm^{3+}, Yb^{3+}, and Er^{3+})] fall in the low-loss telecommunications window between 1250 and 1650 nm. (b) Transmission after 50 km of optical fiber. At visible wavelengths, losses seem prohibitive. In contrast, in the telecommunications window the 10% transmission may be sufficient for quantum networking at a reasonable rate.

Ulanowski, and Reiserer, 2020; Ulanowski, Merkel, and Reiserer, 2022). However, owing to the millisecond-long lifetime of their telecom transition in all studied hosts (Böttger *et al.*, 2006; Weiss *et al.*, 2021; Gritsch *et al.*, 2022; Stevenson *et al.*, 2022), using single dopants in this platform requires resonators with large Purcell enhancement factors, which have only recently been demonstrated (Dibos *et al.*, 2018; Merkel, Ulanowski, and Reiserer, 2020).

Entanglement generation between remote erbium dopants is still an outstanding challenge. The current state in this respect is presented in Sec. III.B.3. In contrast, elementary quantum network links have been achieved in several other platforms. Most notably remote entanglement generation has been demonstrated with Yb^+ (Moehring *et al.*, 2007; Hucul *et al.*, 2015) and Sr^+ (Stephenson *et al.*, 2020) ions, Rb atoms (Hofmann *et al.*, 2012; Ritter *et al.*, 2012), and nitrogen-vacancy (N-*V*) centers in diamond (Bernien *et al.*, 2013). Therefore, these hardware platforms are explained in detail in Secs. III.B.1–III.B.3.

1. Atoms in vacuum

Many pioneering experiments in the field of quantum networks have used atoms trapped in vacuum. Since the first generation of remote entanglement (Moehring *et al.*, 2007), several other experiments have achieved this milestone (Hofmann *et al.*, 2012; Ritter *et al.*, 2012; Hucul *et al.*, 2015; Stephenson *et al.*, 2020; Daiss *et al.*, 2021). By integrating the atoms into optical resonators, high efficiencies and many advanced protocols have been realized (Reiserer and Rempe, 2015), including teleportation (Nölleke *et al.*, 2013; Langenfeld, Welte *et al.*, 2021), quantum memories with single (Specht *et al.*, 2011; Kalb *et al.*, 2015; Brekenfeld *et al.*, 2020) and several atoms (Casabone *et al.*, 2015; Langenfeld *et al.*, 2020), photon-mediated quantum gates (Reiserer *et al.*, 2014; Tiecke *et al.*, 2014; Hacker *et al.*, 2016; Daiss *et al.*, 2021; Dordevic *et al.*, 2021), nondestructive photon (Reiserer, Ritter, and Rempe, 2013; Distante *et al.*, 2021) and photonic qubit detection (Niemietz *et al.*, 2021), and basic quantum repeater nodes (Langenfeld, Thomas *et al.*, 2021). These advances have established trapped atoms as one of the leading experimental platforms for quantum networks.

To use atoms in vacuum as stationary and efficient network nodes, one has to localize them to a subwavelength spot. To this end, tight trapping potentials with trap frequencies on the order of a few hundred kilohertz are typically employed. The atoms are then confined in the Lamb-Dicke regime (Leibfried *et al.*, 2003), where the motional state of the atom only occasionally changes in absorption and emission events. Still, efficient laser recooling is possible using various techniques (Reiserer and Rempe, 2015), leaving the atom in the ground state of the potential (Reiserer *et al.*, 2013).

To implement the required trap, two approaches can be followed: First, the electrical trapping of charged atoms (Leibfried *et al.*, 2003) and, second, optical trapping in far-detuned laser fields (Grimm, Weidemüller, and Ovchinnikov, 2000). Both traps can be integrated with optical resonators in order to enhance the efficiency of spin-photon interactions, as shown in Fig. 9. As several atoms can be loaded to the same trap, quantum network nodes with several qubits can be realized (Casabone *et al.*, 2013; Neuzner *et al.*, 2016). These qubits can be different atomic species to avoid crosstalk during optical addressing and control (Inlek *et al.*, 2017).

When trapped in vacuum, atoms are well isolated from both the environment and one another. Thus, they can exhibit long coherence times. With neutral atoms in optical resonators, encoding the qubit in a magnetic-field-insensitive state has enabled a spin-echo time exceeding 100 ms (Körber *et al.*, 2018), which is already promising for extended quantum networks. Eventually, in deep optical dipole traps the coherence will be limited by scattering of trap photons and by the requirement to periodically recool the atoms. This is avoided in electrical traps, where sympathetic cooling has recently enabled coherence times on the scale of 1 h for Yb^+, which is still far from the fundamental limitations of background gas scattering and hyperfine lifetime (Wang *et al.*, 2021).

Such long coherence times pose no restrictions to the fidelity of single- and two-qubit operations within a node. In addition, most technical limitations can be avoided by careful experimental design, by advanced pulses and pulse sequences

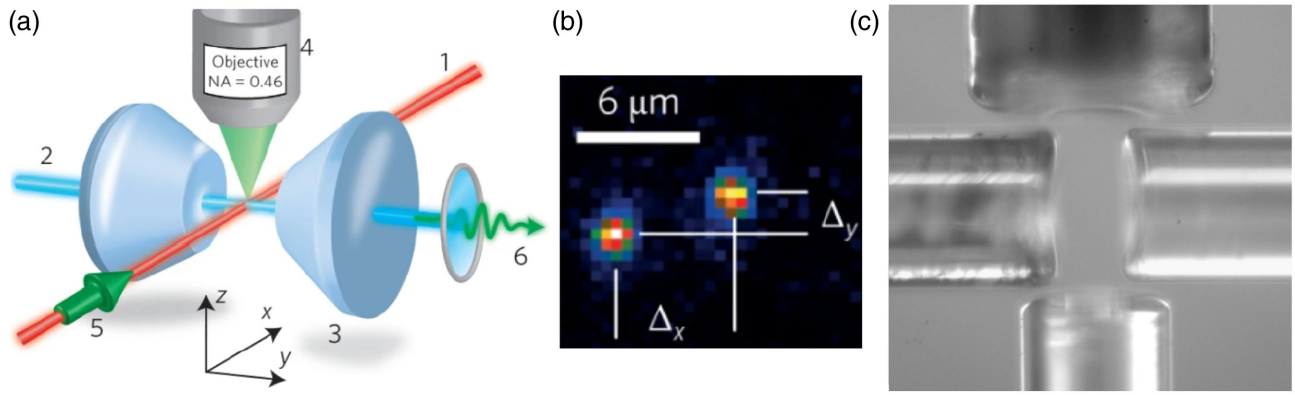

FIG. 9. Trapped-atom quantum network nodes. (a) Schematic of a typical setup. Atoms are trapped in a Fabry-Perot resonator (3) using standing-wave laser fields (1 and 2), and an objective (4) collects scattered light for imaging. (b) Fluorescence image used to determine the number of loaded atoms and their position along x and z. Individual addressing is possible with tightly focused laser beams in order to realize a quantum network node with several stationary qubits. Adapted from Neuzner *et al.*, 2016. (c) Photograph of a crossed-cavity setup of Brekenfeld *et al.* (2020). Each of the two resonators consists of two coated glass fiber end facets with Gaussian depressions generated by laser ablation. A single atom can be coupled simultaneously to both resonators, which facilitates advanced quantum networking protocols.

adapted from nuclear magnetic resonance (Vandersypen and Chuang, 2005), and by optimal control theory (Werschnik and Gross, 2007). In this way, high fidelities [exceeding 99.99% (in the absence of a resonator) (Ballance *et al.*, 2016)] for the preparation of arbitrary single-qubit states have been demonstrated. To this end, the atom is first initialized to a single state by optical pumping. Irradiation of electromagnetic fields at the frequency of the qubit transition can then induce arbitrary rotations. The use of optical rather than microwave fields eases individual addressing of several qubits in the same trap. A more detailed description of the techniques for single-atom control was given by Reiserer and Rempe (2015).

In addition to high-fidelity initialization, faithful readout of the atomic state can be achieved using fluorescence state detection both in free space and in optical resonators. In the latter, as described in Sec. II.C resonator transmission can be used to reduce or even avoid readout-induced heating by photon scattering (Volz *et al.*, 2011).

The implementation of quantum repeaters with dedicated memory and communication qubits also requires one to control several atoms (Casabone *et al.*, 2015; Neuzner *et al.*, 2016) with individual addressing (Langenfeld *et al.*, 2020; Langenfeld, Welte *et al.*, 2021) and local deterministic two-qubit operations. To date high-fidelity gates based on the Coulomb interaction have been achieved even between ions of different species (Negnevitsky *et al.*, 2018; Hughes *et al.*, 2020), with fidelities of 99.8% in the absence of a resonator. For neutral atoms, gates can be implemented via photonic interactions (Welte *et al.*, 2018) or via dipolar coupling in a highly excited Rydberg state (Saffman, Walker, and Mølmer, 2010), enabling entanglement generation fidelities $> 99\%$ in the absence of a resonator (Madjarov *et al.*, 2020). Finally, the realization of quantum networks requires entanglement between remote nodes with high success probabilities η and fidelity F. In free space, values of $\eta = 2 \times 10^{-4}$ and $F = 94\%$ have been demonstrated with trapped ions (Stephenson *et al.*, 2020). Neutral atoms in optical resonators have achieved $\eta = 2\%$ and $F = 85\%$ based on a Raman absorption protocol (Ritter *et al.*, 2012), and $\eta = 0.6\%$ and $F = 79\%$ based on a remote quantum gate protocol (Daiss *et al.*, 2021). As no fundamental limitations have been identified in these experiments, it seems likely that these values can be further improved, based either on the previously used protocols or on novel approaches to heralded qubit storage (Bechler *et al.*, 2018; Brekenfeld *et al.*, 2020). Eventually, exceeding the error-correction threshold of surface codes (Fowler *et al.*, 2012) in a networked topology (Nickerson, Li, and Benjamin, 2013) ($F \gtrapprox 90\%$ for remote entanglement) seems feasible. In this context, the $F = 98\%$ result achieved when one post-selects on the correct atomic state initialization (Ritter *et al.*, 2012) is encouraging.

To summarize, trapped atoms are a leading platform for the implementation of quantum networks and repeaters. The next steps toward the latter will likely involve the development of systems with more individually controlled qubits per node (Casabone *et al.*, 2015; Hucul *et al.*, 2015; Langenfeld *et al.*, 2020; Langenfeld, Welte *et al.*, 2021), potentially with dedicated communication and memory qubits. Compared to the other platforms under study, the main advantage of atoms trapped in vacuum is their excellent isolation, which enables long coherence and operations with exceptional fidelity. However, this comes at the cost of requiring ultrahigh-vacuum and advanced optical setups with precisely stabilized high-power lasers. Albeit such systems have been realized in many laboratories, the implementation of field-deployable quantum network nodes based on trapped atoms is an outstanding engineering challenge.

2. Defect centers in semiconductors

Because of the aforementioned technical overhead required to trap and cool single atoms in vacuum, significant effort has been invested in the search for solid-state alternatives. The first such system that has received considerable attention is the N-V center in diamond. Landmark experiments with this platform include the demonstration of spin-photon entanglement (Togan *et al.*, 2010), remote entanglement

(Bernien *et al.*, 2013) over distances of up to 1.3 km (Hensen *et al.*, 2015), the unconditional teleportation of a quantum state (Pfaff *et al.*, 2014), the distillation of entanglement between remote quantum network nodes (Kalb *et al.*, 2017), the deterministic delivery of remote entanglement (Humphreys *et al.*, 2018), and the realization of a three-node quantum network (Pompili *et al.*, 2021).

These experiments have been facilitated by the notable coherence properties of N-*V* center spins in diamond (Doherty *et al.*, 2013) up to room temperature, which form the basis for many applications in quantum sensing (Degen, Reinhard, and Cappellaro, 2017). When one transfers qubits to the nuclear spin of nearby ^{13}C atoms, coherence can even be preserved for seconds (Maurer *et al.*, 2012). The coupling to phonons prevents the use of N-*V* centers for remote entanglement generation at room temperature, as it leads to fast mixing of the excited state spin (Doherty *et al.*, 2013). Instead, cryogenic operation at a typical temperature of 4 K is required to this end.

At such a temperature, the individual optical transitions of the N-*V* center can be resolved (Batalov *et al.*, 2009). Some of them preserve the spin state well (Tamarat *et al.*, 2008) and can thus be used for single-shot readout with high fidelity, provided the photon collection efficiency is high. This was first achieved (Robledo *et al.*, 2011) by placing the N-*V* center into a solid immersion lens (Hadden *et al.*, 2010). In this way, total internal reflection in high-refractive-index host materials is avoided. The solid immersion lens can be combined with antireflective coatings to enhance the collection efficiency toward the theoretical maximum of 50% when a lens system with a high numerical aperture is used.

Efficient collection also helps increase the rate of remote entanglement by two-photon interference (Bernien *et al.*, 2012; Sipahigil *et al.*, 2012), which typically starts with the generation of spin-photon entanglement at both remote nodes. While initial experiments used polarization qubits (Togan *et al.*, 2010), an alternative scheme based on time-bin qubits (Barrett and Kok, 2005) turned out to be more robust (Bernien *et al.*, 2013), as it comes naturally with the decoupling of magnetic dephasing.

To realize this scheme and prove entanglement by reading the spin state in different bases, ground-state control needs to be implemented. Albeit all-optical control can also be used with defect qubits (Santori *et al.*, 2006; Yale *et al.*, 2013), providing minimal crosstalk in dense systems, experiments typically use microwave pulses for ease of implementation. In the N-*V* center, the combination of a small magnetic bias field with the zero-field splitting of the defect (Doherty *et al.*, 2013) leads to transition frequencies of around 3 GHz, which can be conveniently applied via nearby wires or microwave striplines. In this way, control fidelities of around 99.9% are routinely achieved (Hensen *et al.*, 2015). Such high pulse fidelities also allow for dynamical decoupling with many control pulses to extend the coherence time of the electronic spin beyond 1 s at cryogenic temperature.

This is possible even in samples with natural isotope abundance (Abobeih *et al.*, 2018), where about 99% of the carbon atoms have no nuclear spin. The few remaining ^{13}C spins in proximity to the N-*V* electronic spin can be used as an additional resource for quantum information processing. In particular, they can serve as quantum registers (Dutt *et al.*, 2007; Neumann *et al.*, 2010), potentially with error correction (Waldherr *et al.*, 2014; Cramer *et al.*, 2016), and as robust memory qubits in a quantum network node (Reiserer *et al.*, 2016), as they are decoupled from the optical channels and interact only with adjacent spins. Thus, when one uses tailored sequences, the nuclear spin state is preserved for thousands of entanglement attempts (Kalb *et al.*, 2018). In combination with the recently demonstrated potential for minutelong natural dephasing times (Bartling *et al.*, 2022), this makes nuclear spin registers a unique resource for quantum networks.

For the potential of nuclear spins to be harnessed, they have to be controlled with high fidelity via the hyperfine interaction with the electronic spin. Strongly coupled spins can be controlled via frequency-selective electromagnetic fields (Jelezko *et al.*, 2004; Dutt *et al.*, 2007) but quickly lose their coherence when the electronic spin undergoes a random flip during entanglement generation attempts (Blok *et al.*, 2015). Therefore, the control of spin registers with weaker coupling is preferable. This comes at a cost of slower local operations, whose speed is, however, not a limiting factor in typical long-distance experiments. The required universal control can be achieved with a sequence of microwave pulses (Taminiau *et al.*, 2014), potentially in combination with radio-frequency pulses to enhance the number of controllable spins and further improve the control fidelity (Bradley *et al.*, 2019).

The main challenge in using the N-*V* center in quantum network nodes is the inefficiency of its zero-phonon optical transition (Doherty *et al.*, 2013). Albeit single-photon protocols can substantially improve the rate (Campbell and Benjamin, 2008; Kalb *et al.*, 2017) and thus facilitate repeat-until-success entanglement (Humphreys *et al.*, 2018), for large-distance experiments the achievable rates seem prohibitively low. Therefore, it would be desirable to enhance the emission into the zero-phonon line via the Purcell effect. This was first achieved in nanophotonic resonators (Faraon *et al.*, 2011), but the spectral diffusion of the optical transition observed in these experiments has hindered remote entanglement.

The frequency instability is attributed to charge fluctuations. While the state of the N-*V* center itself can be well controlled (Siyushev *et al.*, 2013; Doi *et al.*, 2014), the Stark effect induces large jumps of the optical transition frequency when changing the state of nearby charge traps. In pure bulk crystals, the effect is small enough to be compensated for by feedback (Robledo *et al.*, 2011; Acosta *et al.*, 2012), but the proximity of charge traps at the interface impedes the use of nanostructured diamond resonators.

A possible solution is to integrate bulk crystals with embedded N-*V* centers into Fabry-Perot resonators with small mode volumes and high finesse. Purcell enhancement has also been demonstrated in such a setting (Riedel *et al.*, 2017). Still, in spite of recent progress (Casabone *et al.*, 2021; Fontana *et al.*, 2021), it has turned out to be difficult for one to achieve the required length stability of a cavity with transversal scanning ability when operating in closed-cycle cryogenic systems (Janitz *et al.*, 2015; Bogdanovic *et al.*, 2017), with

their typically strong vibrations. Instead, positioning individual defects within a rigid tube resonator assembly, as demonstrated with rare-earth dopants (Merkel, Ulanowski, and Reiserer, 2020), may provide a viable solution.

An alternative to such efforts is to use defects other than the N-*V* center. In particular, the absence of a linear Stark shift for defects with inversion symmetry (Macfarlane, 2007) is beneficial for quantum network nodes. Pioneering work used the Si-*V* center in diamond, which has promising optical properties in the negatively charged (Hepp *et al.*, 2014; Rogers *et al.*, 2014) and neutral states (Rose *et al.*, 2018), which both show stable transition frequencies and a comparably large fraction of zero-phonon-line emission. Two-photon interference experiments have demonstrated good photon indistinguishability (Sipahigil *et al.*, 2014), which forms the basis for spin-spin entanglement by detecting photons emitted into a waveguide (Sipahigil *et al.*, 2016). Experiments with photonic-crystal resonators, as shown in Fig. 10, have now paved the way for entanglement and quantum networking experiments (Evans *et al.*, 2018; Nguyen *et al.*, 2019) based on the phase-shift mechanism presented in Fig. 5. Memory-enhanced quantum communication (Bhaskar *et al.*, 2020) and the entanglement of several frequency-multiplexed emitters in the same resonator (Levonian *et al.*, 2022) have been demonstrated in this platform, thereby indicating the key steps required for implementing a quantum repeater; see Fig. 1.

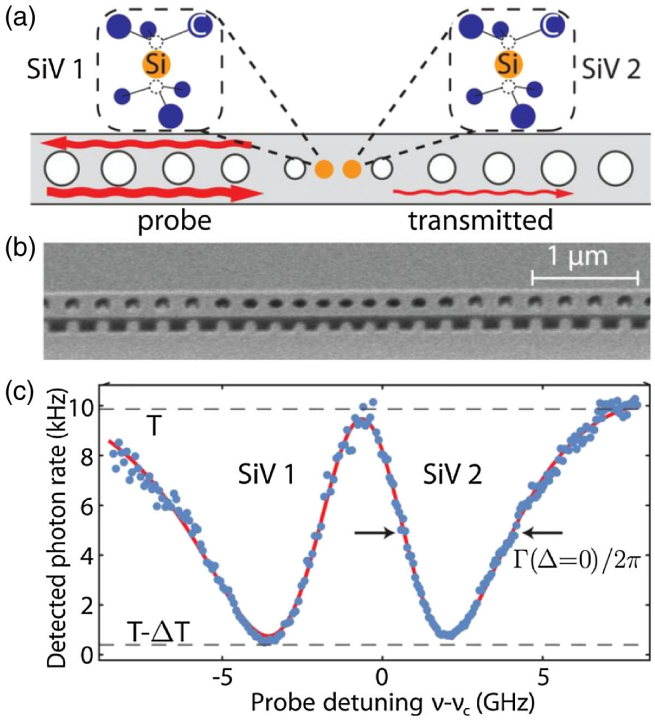

FIG. 10. Quantum network node based on defect centers in diamond. (a) Typical experimental setting. Light is confined along the direction of a waveguide with a triangular cross section using a periodic pattern of holes. Individual defect centers, here two Si-*V* centers, are generated at the field maximum by implantation and annealing. Light is coupled to the resonator via a tapered optical fiber attached to a tapered end of the waveguide (not shown). (b) Scanning electron micrograph of a diamond resonator fabricated by reactive ion etching. (c) Spectral signature of the Si-*V*–resonator coupling. The cavity is tuned such that the probe laser beam is on resonance. At the transition frequencies of two coupled Si-*V* centers, the transmission is almost completely suppressed, indicating a good emitter-resonator coupling, which can be quantified from the broadening of the Si-*V* transition linewidth Γ. Adapted from Evans *et al.*, 2018.

Still, a drawback of negatively charged Si-*V* centers is that sufficient coherence of the ground state has been obtained thus far only at millikelvin temperature (Jahnke *et al.*, 2015; Sukachev *et al.*, 2017; Becker *et al.*, 2018) or in strained devices (Stas *et al.*, 2022). As an alternative, other group-IV defects may also operate at higher temperatures, such as the neutral Si-*V* center (Rose *et al.*, 2018) and the Sn-*V* center (Trusheim *et al.*, 2020; Rugar *et al.*, 2021). They may thus be favorable for enhancing the prospect of upscaling. In this respect, the difficulty of growing pure diamond samples on a wafer scale (albeit favorable for the jewelry industry) may be an obstacle unless hybrid integration is used (Wan *et al.*, 2020). This challenge is less pronounced in other large-band-gap semiconductors, such as silicon carbide. In addition, in this material a large number of defects with promising properties have been identified. Recent overviews were given by Atatüre *et al.* (2018) and Wolfowicz *et al.* (2021). In particular, silicon-vacancy centers (Riedel *et al.*, 2012; Nagy *et al.*, 2019) have demonstrated the generation of indistinguishable photons (Morioka *et al.*, 2020) with high efficiency (Lukin, Guidry, and Vučković, 2020; Babin *et al.*, 2022), making SiC a promising candidate for the scaling of quantum networks. Note, however, that most defects in SiC and diamond emit light at frequencies where the transmission of optical fibers is moderate, as shown in Fig. 8. Therefore, photon conversion to the telecom band will be required to bridge global distances. Still, there are several emitters in the *O* band around 1300 nm in SiC (J.-F. Wang *et al.*, 2020; Wolfowicz *et al.*, 2020) and silicon (Bergeron *et al.*, 2020; Durand *et al.*, 2021) that may be used over larger distances without wavelength conversion.

3. Rare-earth dopants

In spite of the well-developed quantum network nodes based on trapped atoms and defects in large-band-gap semiconductors, the search for qubit systems with improved properties has not come to an end. In recent years, a third promising platform has emerged in this context: crystals with rare-earth dopants, typically in the triply ionized state. These emitters exhibit optical transitions between electronic states in the inner $4f$ shell (Thiel, Böttger, and Cone, 2011), which are surrounded by filled $5s$ and $5p$ shells. The electrons in these outer orbitals shield the electric field of neighboring atoms in the crystal to a significant degree. Thus, the crystal field can be treated as a small perturbation to the energy levels of the free ion (Liu and Jacquier, 2005) such that the optical transition frequencies are almost independent of the host crystal. For one of the rare-earth dopants, erbium, these transitions fall within the telecommunications window around 1550 nm. This not only serves as the basis for erbium-doped fiber lasers and amplifiers that are widespread in classical networks but also makes this emitter an interesting candidate for quantum networks. In this context, the coherence of the optical

transitions is paramount. Because of the shielding effect, at cryogenic temperature the coupling to phonons plays a negligible role in most hosts, and optical coherence of several milliseconds is obtained in some systems (Böttger *et al.*, 2006), the longest span observed in any solid.

Decoherence rates can also be extremely low in the ground state, where the precise value depends on the dopant, host crystal, and magnetic field (Thiel, Böttger, and Cone, 2011). In some systems, spin lifetimes of several weeks are observed, a finding that forms the basis for the realization of quantum memories with exceptional lifetime of several hours (Zhong *et al.*, 2015). In this context, the ideal host crystal exhibits a high Debye temperature, has a large band gap and a low impurity concentration, and is free of nuclear magnetic moments (Atatüre *et al.*, 2018; Zhong and Goldner, 2019; Wolfowicz *et al.*, 2021). In addition, the dopants should be integrated at a well-defined lattice site without generating too much strain or fluctuating charge traps. Finally, the crystal field levels should be well split, which reduces phononic relaxation at a given temperature (Liu and Jacquier, 2005; Wolfowicz *et al.*, 2021).

A common host crystal that fulfills most of these requirements is yttrium orthosilicate (YSO). Other materials can also be favorably used, depending on the application. In many hosts, the crystal field splittings are on the order of a few terahertz, such that only the lowest manifold is significantly populated at liquid helium temperature. Upon optical excitation and decay, higher lying crystal field levels can be populated, but they quickly relax to the ground state through phonon emission.

The rare-earth dopants can be further classified into Kramers (typically Ce, Nd, Er, and Yb) and non-Kramers ions (Pr, Eu, and Tm) with odd and even numbers of $4f$ electrons, respectively. The degeneracy of the spin degree of freedom of Kramers ions with their single unpaired electron is lifted in an external magnetic field. The electronic state can then be modeled as a two-level system, i.e., an ideal qubit, in both the ground and optically excited state manifolds (Thiel, Böttger, and Cone, 2011). Because of the large angular momentum of electrons in the $4f$ shell, the effective g factor can be large. This not only makes Kramers ions well suited for molecular magnets (Coronado, 2020) but could also allow for sensitive magnetic-field sensors, microwave quantum memories (Probst *et al.*, 2015), and microwave-to-optical transducers (Bartholomew *et al.*, 2020). However, the strong and anisotropic interactions between Kramers dopants pose a challenge in this respect, as they can limit the spin lifetime (Car *et al.*, 2019) and coherence even when tailored dynamical decoupling sequences are applied (Merkel, Cova Fariña, and Reiserer, 2021).

Thus, using the electronic spin of Kramers dopants in quantum network nodes seems promising only at ultralow concentrations (Cova Fariña *et al.*, 2021; Dantec *et al.*, 2021). As an alternative, long-lived quantum states can be encoded in the nuclear rather than electronic spin of the dopant (Ortu *et al.*, 2018; Rančić *et al.*, 2018; Kindem *et al.*, 2020; Rakonjac *et al.*, 2020; Ruskuc *et al.*, 2022). To this end, the electronic spin of Kramers dopants can also be frozen to the ground state at low temperatures ($\lesssim 2$ K) and with large magnetic fields ($\gtrsim 3$ T). In this way, secondlong coherence has been obtained (Rančić *et al.*, 2018), and further improvement is expected in other hosts or at lower temperatures.

In non-Kramers systems with their quenched electronic magnetic moment, even longer coherence times have been achieved, with the current record of 6 h for the hyperfine states in Eu:YSO (Zhong *et al.*, 2015). As this host exhibits a large number of nuclear spins, achieving such long coherence relies on two effects: First, the direction and amplitude of an external magnetic field is tuned such that the hyperfine transition frequency is first order insensitive to magnetic-field fluctuations (Langer *et al.*, 2005), which is possible even at zero external field with Kramers dopants (Ortu *et al.*, 2018; Kindem *et al.*, 2020; Rakonjac *et al.*, 2020). Second, the dynamics of the nuclear spin bath is slowed down in the "frozen core" that is generated around a rare-earth impurity by its magnetic moment (Geschwind, 1972). The detrimental effect of the remaining slow nuclear spin bath dynamics, and other effects such as temperature drifts, can be alleviated using dynamical decoupling (Suter and Álvarez, 2016).

Using the aforementioned techniques, exceptional coherence of both ground-state and optical transitions can be obtained, thereby offering great promise for the implementation of quantum networks. There is only one major challenge in this respect: The protected intra-$4f$ transitions of the rare-earth dopants have only weak dipole moments. In free space they are forbidden by symmetry, and even in crystals the observed lifetimes are typically in the range of milliseconds. For this reason, early quantum network experiments with rare-earth dopants have used large ensembles, as discussed in Sec. II.E.3. This has allowed for the implementation of efficient and broadband quantum memories (Lvovsky, Sanders, and Tittel, 2009; Afzelius, Gisin, and de Riedmatten, 2015) that can store entangled photons (Clausen *et al.*, 2011; Saglamyurek *et al.*, 2011) and offer a large multiplexing capacity (Tittel *et al.*, 2010; Afzelius, Gisin, and de Riedmatten, 2015) that can be utilized in tailored quantum repeater protocols (Sinclair *et al.*, 2014).

Still, in spite of low count rates, single dopants (Kolesov *et al.*, 2012; Utikal *et al.*, 2014) and nuclear spins in their proximity (Kornher *et al.*, 2020) have been detected. To use such systems for quantum networks, improving the spin readout and photon generation speed is highly desirable. This can be achieved by integrating the emitters into optical resonators. Recent experiments with nanophotonic structures have resolved single dopants (Dibos *et al.*, 2018; Zhong *et al.*, 2018; Xia *et al.*, 2022), implemented single-shot readout (Kindem *et al.*, 2020; Raha *et al.*, 2020) and nuclear spin registers (Ruskuc *et al.*, 2022), and demonstrated frequency-domain multiplexing and the simultaneous control of several dopants (Chen *et al.*, 2020; Ulanowski, Merkel, and Reiserer, 2022). In these experiments, Purcell enhancement factors between 100 and 1000 have been achieved, thus reducing the optical lifetime to a few microseconds. This is short compared to the time it takes to transmit photons to remote quantum network nodes, so it will not limit the achievable rate in remote entanglement experiments. For this basic quantum network functionality to be implemented, the transition frequency of the emitters has to be stable, which is difficult

in nanostructures as the proximity of charge traps at the interface can lead to considerable spectral diffusion linewidths. Using Er:YSO in proximity to a nanophotonic silicon resonator, ∼10 MHz have been measured (Dibos *et al.*, 2018). In sites that lack a linear Stark shift (Macfarlane, 2007), narrower lines have been observed: for instance, ∼1 MHz with yttrium orthovanadate doped with Yb, which is close to the lifetime limit in this experiment (Kindem *et al.*, 2020).

Another approach for obtaining large Purcell enhancement is the integration of rare-earth dopants into Fabry-Perot resonators. In contrast to experiments with nanocrystals (Casabone *et al.*, 2018, 2021), the use of polished crystalline membranes allows for considerable Purcell enhancement while allowing the optical coherence and spectral stability observed in bulk materials to be preserved (Merkel, Ulanowski, and Reiserer, 2020). Recent progress in this setup is shown in Figs. 11(c) and 11(d) (Ulanowski, Merkel, and Reiserer, 2022). When one operates at a large detuning from the center of the inhomogeneous line, single erbium dopants are spectrally resolved, albeit $\sim 10^7$ dopants fall within the cavity mode and $\sim 10^4$ dopants fall within a diffraction-limited volume. The observed Purcell enhancement reaches ∼70-fold, depending on the position of the dopants in the standing-wave cavity mode [Fig. 11(b)]. The frequency of the individual peaks is stable over several hours [Fig. 11(d)], with an average FWHM of < 0.2 MHz. These narrow lines allow for resolving and controlling approximately 10^3 dopants when fast resonator tuning (Casabone *et al.*, 2021) is implemented.

The remaining broadening is explained by the coupling of the electronic spin to the nuclear spin bath (Merkel, 2021). Thus, a considerable improvement is expected when one uses the isotope ^{167}Er at a magnetic-field insensitive point (Ortu *et al.*, 2018; Rakonjac *et al.*, 2020). Alternatively, different host materials that have only a small abundance of nuclear magnetic moments can be considered. Recently studied materials include TiO_2 (Phenicie *et al.*, 2019), calcium tungstate (Dantec *et al.*, 2021), and crystalline silicon (Yin *et al.*, 2013; Berkman *et al.*, 2021; Weiss *et al.*, 2021;

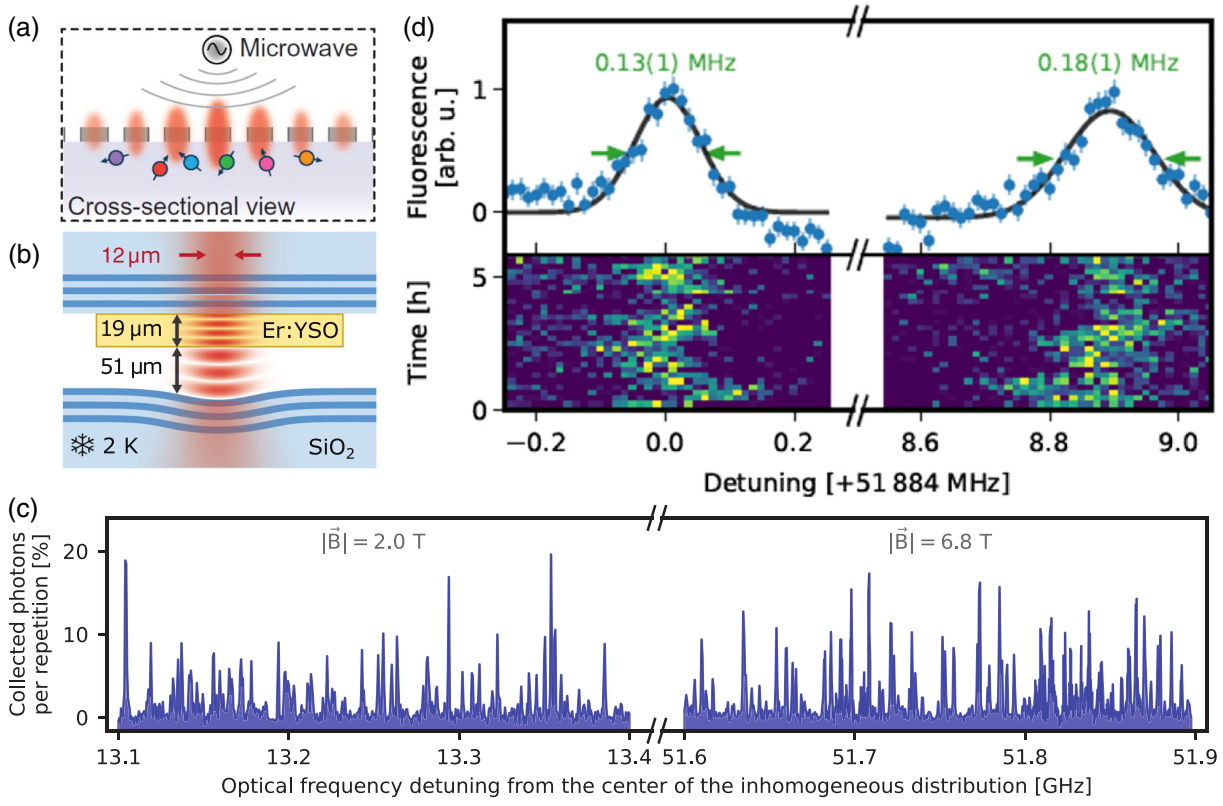

FIG. 11. Quantum network node based on rare-earth dopants. (a) Cross-sectional view of a silicon (gray rectangles) photonic-crystal resonator, fabricated on top of a YSO crystal (purple circle) using a stamping technique. Individual rare-earth dopants (colored spin symbols) in the evanescent field of the resonator (red ellipsoids) can be addressed individually via their differing optical transition frequencies. From Chen *et al.*, 2020. (b) Fabry-Perot resonator. Rare-earth dopants are integrated into a 19 μm thin YSO membrane placed between two dielectric mirrors (light and dark blue layers), one of which has a depression to form a stable cavity mode (red ellipsoids). From Ulanowski, Merkel, and Reiserer, 2022. (c) Spectral multiplexing. The resonant emission frequency of the dopants [colored spin symbols in (a)] depends on the local crystalline environment and can thus differ by several gigahertz, with a typical FWHM inhomogeneous linewidth of a few hundred megahertz. Scanning the optical frequency detuning of the excitation laser thus enables the spectral resolution and coherent control of hundreds of individual dopants (fluorscence peaks) in a few-wavelength-scale volume. (d) Spectral stability of two resonator-integrated erbium dopants in YSO, measured at the same time. Only small, uncorrelated fluctuations of the emission maximum (bottom panels) are observed over several hours. The time-integrated spectral diffusion linewidth (top panel) of ∼0.2 MHz is consistent with the expected broadening caused by the Y nuclear spin bath, and may thus be reduced or eliminated in other host materials. From Ulanowski, Merkel, and Reiserer, 2022.

Gritsch *et al.*, 2022). Crystalline silicon seems particularly promising, as isotopically purified material can be epitaxially grown by chemical vapor deposition (CVD) on a wafer scale (Mazzocchi *et al.*, 2019).

Recent experiments in CVD silicon with natural isotope abundance have revealed narrow inhomogeneous (< 1 GHz) and homogeneous ($\lesssim 20$ kHz) linewidths of erbium dopants at specific lattice sites (Gritsch *et al.*, 2022), on a par with established host materials such as YSO. Because of its high refractive index (de Vries and Lagendijk, 1998), the radiative lifetime in silicon can be almost 100 times shorter than in YSO, thus enhancing the expected rate in quantum network experiments. When isotopically purified membranes are integrated into Fabry-Perot resonators, a large number of dopants with negligible spectral diffusion may be controlled. Combined with its emission at telecommunication frequency and the prospect for secondlong ground-state coherence (Rančić *et al.*, 2018), this makes such systems a promising platform for the implementation of global quantum networks and quantum repeaters.

IV. SUMMARY AND OUTLOOK

The integration of single emitters into low-loss optical resonators has unique potential for the realization of scalable quantum networks. The first steps in this direction have been taken in several experimental platforms, which have demonstrated the successful initialization, control, readout, and remote entanglement of spin qubits based on efficient spin-photon interfaces. Still, scaling up the demonstrated elementary quantum links to a network with many nodes that are distributed over global distances poses a formidable challenge. While many concepts that allow for such networks have been developed (Muralidharan *et al.*, 2016; Wehner, Elkouss, and Hanson, 2018), the experimental requirements of high efficiency and almost 100% fidelity are difficult to achieve in all investigated physical platforms and will therefore require a considerable engineering effort. Still, even with present experimental imperfections the realization of a prototype quantum repeater seems within reach (Rozpedek *et al.*, 2018).

Using such systems outside of the lab, such as in a global communication scenario, will be possible only if the devices are robust and cost effective. Thus, the integration of the presented quantum network nodes with on-chip photonics (J. Wang *et al.*, 2020) will likely receive growing attention. Based on the current optical fiber infrastructure, the maximum separation of quantum repeater nodes will have to be on the order of 100 km, a distance after which 99% of the photons have been lost. Covering continental distances with an equally spaced network of high-vacuum chambers or closed-cycle ^{4}He cryostats at such spacing seems feasible. This would be sufficient to provide users that have limited quantum processing capacity, such as only photodetectors and phase or polarization modulators, access to quantum network resources. Bridging the gaps between continents, however, seems to be more difficult and may favor the use of quantum satellites (Yin *et al.*, 2017) or drones (Liu *et al.*, 2020) rather than fiber-based links.

Going beyond point-to-point connections to generate entangled states of many nodes will require the implementation of entanglement distillation or quantum error correction. In the latter, current topological codes allow for error probabilities of a few percent (Fowler *et al.*, 2012; Nickerson, Li, and Benjamin, 2013) but then require an impractical overhead. Therefore, increasing the fidelity of remote entanglement far beyond what is achieved in current experiments will be paramount. To this end, the spectral stability of the emitters and resonators will have to be improved, particularly for solid-state qubits. Alternatively, much larger Purcell enhancement may be targeted.

If successful, the implementation of large quantum networks will open the door for novel fundamental tests (Brunner *et al.*, 2014; Pikovski *et al.*, 2015) at the forefront of contemporary quantum science. In addition, they will enable numerous applications. In particular, the upscaling of quantum computers may be based on a modular architecture (Awschalom *et al.*, 2013; Monroe and Kim, 2013; Kinos *et al.*, 2021), similar to the distribution of information processing among different components in classical high-performance computers and data centers. To this end, boosting the rate of remote entanglement to approach that of local quantum gates is highly desirable. This will further stimulate the research into optimized materials systems and resonator-integrated qubit platforms in the coming decades.

ACKNOWLEDGMENTS

I acknowledge discussions with Andreas Gritsch and Benjamin Merkel, as well as funding from the European Research Council (ERC) under the European Union's Horizon 2020 research and innovation program (Grant Agreement No. 757772), and from the Deutsche Forschungsgemeinschaft (DFG, German Research Foundation) under Germany's Excellence Strategy EXC-2111–390814868.

REFERENCES

Abobeih, M. H., J. Cramer, M. A. Bakker, N. Kalb, M. Markham, D. J. Twitchen, and T. H. Taminiau, 2018, Nat. Commun. **9**, 2552.
Acosta, V. M., *et al.*, 2012, Phys. Rev. Lett. **108**, 206401.
Afzelius, M., N. Gisin, and H. de Riedmatten, 2015, Phys. Today **68**, No. 12, 42.
Afzelius, M., and C. Simon, 2010, Phys. Rev. A **82**, 022310.
Aoki, T., B. Dayan, E. Wilcut, W. P. Bowen, A. S. Parkins, T. J. Kippenberg, K. J. Vahala, and H. J. Kimble, 2006, Nature (London) **443**, 671.
Asano, T., and S. Noda, 2018, Proc. IEEE **106**, 2183.
Asano, T., Y. Ochi, Y. Takahashi, K. Kishimoto, and S. Noda, 2017, Opt. Express **25**, 1769.
Atatüre, M., D. Englund, N. Vamivakas, S.-Y. Lee, and J. Wrachtrup, 2018, Nat. Rev. Mater. **3**, 38.
Awschalom, D. D., L. C. Bassett, A. S. Dzurak, E. L. Hu, and J. R. Petta, 2013, Science **339**, 1174.
Awschalom, D. D., R. Hanson, J. Wrachtrup, and B. B. Zhou, 2018, Nat. Photonics **12**, 516.
Babin, C., *et al.*, 2022, Nat. Mater. **21**, 67.
Ballance, C. J., T. P. Harty, N. M. Linke, M. A. Sepiol, and D. M. Lucas, 2016, Phys. Rev. Lett. **117**, 060504.
Barrett, S. D., and P. Kok, 2005, Phys. Rev. A **71**, 060310.
Bartholomew, J. G., J. Rochman, T. Xie, J. M. Kindem, A. Ruskuc, I. Craiciu, M. Lei, and A. Faraon, 2020, Nat. Commun. **11**, 3266.

Bartling, H. P., M. H. Abobeih, B. Pingault, M. J. Degen, S. J. H. Loenen, C. E. Bradley, J. Randall, M. Markham, D. J. Twitchen, and T. H. Taminiau, 2022, Phys. Rev. X **12**, 011048.

Barz, S., E. Kashefi, A. Broadbent, J. F. Fitzsimons, A. Zeilinger, and P. Walther, 2012, Science **335**, 303.

Batalov, A., V. Jacques, F. Kaiser, P. Siyushev, P. Neumann, L. J. Rogers, R. L. McMurtrie, N. B. Manson, F. Jelezko, and J. Wrachtrup, 2009, Phys. Rev. Lett. **102**, 195506.

Bechler, O., *et al.*, 2018, Nat. Phys. **14**, 996.

Becker, J. N., B. Pingault, D. Groß, M. Gündoğan, N. Kukharchyk, M. Markham, A. Edmonds, M. Atatüre, P. Bushev, and C. Becher, 2018, Phys. Rev. Lett. **120**, 053603.

Bennett, C. H., G. Brassard, S. Popescu, B. Schumacher, J. A. Smolin, and W. K. Wootters, 1996, Phys. Rev. Lett. **76**, 722; **78**, 2031(E) (1997).

Bergeron, L., C. Chartrand, A. T. K. Kurkjian, K. J. Morse, H. Riemann, N. V. Abrosimov, P. Becker, H.-J. Pohl, M. L. W. Thewalt, and S. Simmons, 2020, PRX Quantum **1**, 020301.

Berkman, I. R., *et al.*, 2021, arXiv:2108.07090.

Bernien, H., L. Childress, L. Robledo, M. Markham, D. Twitchen, and R. Hanson, 2012, Phys. Rev. Lett. **108**, 043604.

Bernien, H., *et al.*, 2013, Nature (London) **497**, 86.

Bhaskar, M. K., *et al.*, 2020, Nature (London) **580**, 60.

Blinov, B. B., D. L. Moehring, L.-M. Duan, and C. Monroe, 2004, Nature (London) **428**, 153.

Blok, M. S., N. Kalb, A. Reiserer, T. H. Taminiau, and R. Hanson, 2015, Faraday Discuss. **184**, 173.

Bochmann, J., M. Mücke, C. Guhl, S. Ritter, G. Rempe, and D. L. Moehring, 2010, Phys. Rev. Lett. **104**, 203601.

Bochmann, J., M. Mücke, G. Langfahl-Klabes, C. Erbel, B. Weber, H. P. Specht, D. L. Moehring, and G. Rempe, 2008, Phys. Rev. Lett. **101**, 223601.

Bock, M., P. Eich, S. Kucera, M. Kreis, A. Lenhard, C. Becher, and J. Eschner, 2018, Nat. Commun. **9**, 1998.

Bogaerts, W., P. D. Heyn, T. V. Vaerenbergh, K. D. Vos, S. K. Selvaraja, T. Claes, P. Dumon, P. Bienstman, D. V. Thourhout, and R. Baets, 2012, Laser Photonics Rev. **6**, 47.

Bogdanovic, S., *et al.*, 2017, Appl. Phys. Lett. **110**, 171103.

Boozer, A. D., A. Boca, R. Miller, T. E. Northup, and H. J. Kimble, 2007, Phys. Rev. Lett. **98**, 193601.

Borregaard, J., P. Kómár, E. M. Kessler, A. S. Sørensen, and M. D. Lukin, 2015, Phys. Rev. Lett. **114**, 110502.

Borregaard, J., H. Pichler, T. Schröder, M. D. Lukin, P. Lodahl, and A. S. Sørensen, 2020, Phys. Rev. X **10**, 021071.

Borregaard, J., A. S. Sørensen, and P. Lodahl, 2019, Adv. Quantum Technol. **2**, 1800091.

Böttger, T., C. W. Thiel, Y. Sun, and R. L. Cone, 2006, Phys. Rev. B **73**, 075101.

Bradley, C. E., J. Randall, M. H. Abobeih, R. C. Berrevoets, M. J. Degen, M. A. Bakker, M. Markham, D. J. Twitchen, and T. H. Taminiau, 2019, Phys. Rev. X **9**, 031045.

Brekenfeld, M., D. Niemietz, J. D. Christesen, and G. Rempe, 2020, Nat. Phys. **16**, 647.

Briegel, H. J., D. E. Browne, W. Dür, R. Raussendorf, and M. Van den Nest, 2009, Nat. Phys. **5**, 19.

Briegel, H.-J., W. Dür, J. I. Cirac, and P. Zoller, 1998, Phys. Rev. Lett. **81**, 5932.

Brunner, N., D. Cavalcanti, S. Pironio, V. Scarani, and S. Wehner, 2014, Rev. Mod. Phys. **86**, 419.

Buhrman, H., R. Cleve, S. Massar, and R. de Wolf, 2010, Rev. Mod. Phys. **82**, 665.

Cabrillo, C., J. I. Cirac, P. García-Fernández, and P. Zoller, 1999, Phys. Rev. A **59**, 1025.

Calsamiglia, J., and N. Lütkenhaus, 2001, Appl. Phys. B **72**, 67.

Campbell, E. T., and S. C. Benjamin, 2008, Phys. Rev. Lett. **101**, 130502.

Car, B., L. Veissier, A. Louchet-Chauvet, J.-L. Le Gouët, and T. Chanelière, 2019, Phys. Rev. B **100**, 165107.

Casabone, B., J. Benedikter, T. Hümmer, F. Oehl, K. de O. Lima, T. W. Hänsch, A. Ferrier, P. Goldner, H. de Riedmatten, and D. Hunger, 2018, New J. Phys. **20**, 095006.

Casabone, B., C. Deshmukh, S. Liu, D. Serrano, A. Ferrier, T. Hümmer, P. Goldner, D. Hunger, and H. de Riedmatten, 2021, Nat. Commun. **12**, 3570.

Casabone, B., K. Friebe, B. Brandstätter, K. Schüppert, R. Blatt, and T. E. Northup, 2015, Phys. Rev. Lett. **114**, 023602.

Casabone, B., A. Stute, K. Friebe, B. Brandstätter, K. Schüppert, R. Blatt, and T. E. Northup, 2013, Phys. Rev. Lett. **111**, 100505.

Chang, D. E., V. Vuletić, and M. D. Lukin, 2014, Nat. Photonics **8**, 685.

Chen, S., M. Raha, C. M. Phenicie, S. Ourari, and J. D. Thompson, 2020, Science **370**, 592.

Chen, W., K. M. Beck, R. Bücker, M. Gullans, M. D. Lukin, H. Tanji-Suzuki, and V. Vuletić, 2013, Science **341**, 768.

Chew, X., G. Zhou, F. S. Chau, J. Deng, X. Tang, and Y. C. Loke, 2010, Opt. Lett. **35**, 2517.

Choi, K. S., A. Goban, S. B. Papp, S. J. van Enk, and H. J. Kimble, 2010, Nature (London) **468**, 412.

Chou, C. W., H. de Riedmatten, D. Felinto, S. V. Polyakov, S. J. van Enk, and H. J. Kimble, 2005, Nature (London) **438**, 828.

Cirac, J. I., P. Zoller, H. J. Kimble, and H. Mabuchi, 1997, Phys. Rev. Lett. **78**, 3221.

Clausen, C., I. Usmani, F. Bussières, N. Sangouard, M. Afzelius, H. de Riedmatten, and N. Gisin, 2011, Nature (London) **469**, 508.

Cohen-Tannoudji, C., J. Dupont-Roc, and G. Grynberg, 1989, *Photons and Atoms: Introduction to Quantum Electrodynamics* (John Wiley & Sons, New York).

Colombe, Y., T. Steinmetz, G. Dubois, F. Linke, D. Hunger, and J. Reichel, 2007, Nature (London) **450**, 272.

Coronado, E., 2020, Nat. Rev. Mater. **5**, 87.

Cova Fariña, P., B. Merkel, N. Herrera Valencia, P. Yu, A. Ulanowski, and A. Reiserer, 2021, Phys. Rev. Applied **15**, 064028.

Covey, J. P., A. Sipahigil, S. Szoke, N. Sinclair, M. Endres, and O. Painter, 2019, Phys. Rev. Applied **11**, 034044.

Cramer, J., N. Kalb, M. A. Rol, B. Hensen, M. S. Blok, M. Markham, D. J. Twitchen, R. Hanson, and T. H. Taminiau, 2016, Nat. Commun. **7**, 11526.

Daiss, S., S. Langenfeld, S. Welte, E. Distante, P. Thomas, L. Hartung, O. Morin, and G. Rempe, 2021, Science **371**, 614.

Dantec, M. L., *et al.*, 2021, Sci. Adv. **7**, eabj9786.

Degen, C. L., F. Reinhard, and P. Cappellaro, 2017, Rev. Mod. Phys. **89**, 035002.

De Greve, K., *et al.*, 2012, Nature (London) **491**, 421.

Devitt, S. J., W. J. Munro, and K. Nemoto, 2013, Rep. Prog. Phys. **76**, 076001.

de Vries, P., and A. Lagendijk, 1998, Phys. Rev. Lett. **81**, 1381.

Dibos, A. M., M. Raha, C. M. Phenicie, and J. D. Thompson, 2018, Phys. Rev. Lett. **120**, 243601.

Distante, E., S. Daiss, S. Langenfeld, L. Hartung, P. Thomas, O. Morin, G. Rempe, and S. Welte, 2021, Phys. Rev. Lett. **126**, 253603.

Doherty, M. W., N. B. Manson, P. Delaney, F. Jelezko, J. Wrachtrup, and L. C. L. Hollenberg, 2013, Phys. Rep. **528**, 1.

Doi, Y., *et al.*, 2014, Phys. Rev. X **4**, 011057.

Dordevic, T., P. Samutpraphoot, P. L. Ocola, H. Bernien, B. Grinkemeyer, I. Dimitrova, V. Vuletić, and M. D. Lukin, 2021, Science **373**, 1511.

Duan, L.-M., and H. J. Kimble, 2004, Phys. Rev. Lett. **92**, 127902.
Duan, L.-M., M. D. Lukin, J. I. Cirac, and P. Zoller, 2001, Nature (London) **414**, 413.
Duan, L.-M., and C. Monroe, 2010, Rev. Mod. Phys. **82**, 1209.
Durand, A., *et al.*, 2021, Phys. Rev. Lett. **126**, 083602.
Dutt, M. V. G., L. Childress, L. Jiang, E. Togan, J. Maze, F. Jelezko, A. S. Zibrov, P. R. Hemmer, and M. D. Lukin, 2007, Science **316**, 1312.
Ekert, A., and R. Renner, 2014, Nature (London) **507**, 443.
Evans, R. E., *et al.*, 2018, Science **362**, 662.
Faraon, A., P. E. Barclay, C. Santori, K.-M. C. Fu, and R. G. Beausoleil, 2011, Nat. Photonics **5**, 301.
Firstenberg, O., T. Peyronel, Q.-Y. Liang, A. V. Gorshkov, M. D. Lukin, and V. Vuletić, 2013, Nature (London) **502**, 71.
Fischer, K. A., L. Hanschke, J. Wierzbowski, T. Simmet, C. Dory, J. J. Finley, J. Vučković, and K. Müller, 2017, Nat. Phys. **13**, 649.
Fitzsimons, J. F., 2017, npj Quantum Inf. **3**, 23.
Fontana, Y., R. Zifkin, E. Janitz, C. D. Rodríguez Rosenblueth, and L. Childress, 2021, Rev. Sci. Instrum. **92**, 053906.
Fowler, A. G., M. Mariantoni, J. M. Martinis, and A. N. Cleland, 2012, Phys. Rev. A **86**, 032324.
Gao, W. B., A. Imamoglu, H. Bernien, and R. Hanson, 2015, Nat. Photonics **9**, 363.
Georgescu, I. M., S. Ashhab, and F. Nori, 2014, Rev. Mod. Phys. **86**, 153.
Geschwind, S., 1972, Ed., *Electron Paramagnetic Resonance* (Springer, New York).
Gisin, N., and R. Thew, 2007, Nat. Photonics **1**, 165.
Gorshkov, A. V., A. André, M. D. Lukin, and A. S. Sørensen, 2007, Phys. Rev. A **76**, 033804.
Gottesman, D., T. Jennewein, and S. Croke, 2012, Phys. Rev. Lett. **109**, 070503.
Grimm, R., M. Weidemüller, and Y. B. Ovchinnikov, 2000, in *Advances In Atomic, Molecular, and Optical Physics*, Vol. 42 (Academic Press, New York), pp. 95–170.
Gritsch, A., L. Weiss, J. Früh, S. Rinner, and A. Reiserer, 2022, Phys. Rev. X **12**, 041009.
Gulati, G. K., H. Takahashi, N. Podoliak, P. Horak, and M. Keller, 2017, Sci. Rep. **7**, 5556.
Hacker, B., S. Welte, G. Rempe, and S. Ritter, 2016, Nature (London) **536**, 193.
Hadden, J. P., J. P. Harrison, A. C. Stanley-Clarke, L. Marseglia, Y.-L. D. Ho, B. R. Patton, J. L. O'Brien, and J. G. Rarity, 2010, Appl. Phys. Lett. **97**, 241901.
Hammerer, K., A. S. Sørensen, and E. S. Polzik, 2010, Rev. Mod. Phys. **82**, 1041.
Haroche, S., and J.-M. Raimond, 2013, *Exploring the Quantum: Atoms, Cavities, and Photons* (Oxford University Press, Oxford).
Heller, L., P. Farrera, G. Heinze, and H. de Riedmatten, 2020, Phys. Rev. Lett. **124**, 210504.
Hensen, B., *et al.*, 2015, Nature (London) **526**, 682.
Hepp, C., *et al.*, 2014, Phys. Rev. Lett. **112**, 036405.
Hofmann, H. F., K. Kojima, S. Takeuchi, and K. Sasaki, 2003, J. Opt. B **5**, 218.
Hofmann, J., M. Krug, N. Ortegel, L. Gérard, M. Weber, W. Rosenfeld, and H. Weinfurter, 2012, Science **337**, 72.
Hong, C. K., Z. Y. Ou, and L. Mandel, 1987, Phys. Rev. Lett. **59**, 2044.
Hu, S., M. Khater, R. Salas-Montiel, E. Kratschmer, S. Engelmann, W. M. J. Green, and S. M. Weiss, 2018, Sci. Adv. **4**, eaat2355.
Hucul, D., I. V. Inlek, G. Vittorini, C. Crocker, S. Debnath, S. M. Clark, and C. Monroe, 2015, Nat. Phys. **11**, 37.
Hughes, A. C., V. M. Schäfer, K. Thirumalai, D. P. Nadlinger, S. R. Woodrow, D. M. Lucas, and C. J. Ballance, 2020, Phys. Rev. Lett. **125**, 080504.
Humphreys, P. C., N. Kalb, J. P. J. Morits, R. N. Schouten, R. F. L. Vermeulen, D. J. Twitchen, M. Markham, and R. Hanson, 2018, Nature (London) **558**, 268.
Hunger, D., C. Deutsch, R. J. Barbour, R. J. Warburton, and J. Reichel, 2012, AIP Adv. **2**, 012119.
Inlek, I. V., C. Crocker, M. Lichtman, K. Sosnova, and C. Monroe, 2017, Phys. Rev. Lett. **118**, 250502.
Jahnke, K. D., A. Sipahigil, J. M. Binder, M. W. Doherty, M. Metsch, L. J. Rogers, N. B. Manson, M. D. Lukin, and F. Jelezko, 2015, New J. Phys. **17**, 043011.
Janitz, E., M. K. Bhaskar, and L. Childress, 2020, Optica **7**, 1232.
Janitz, E., M. Ruf, M. Dimock, A. Bourassa, J. Sankey, and L. Childress, 2015, Phys. Rev. A **92**, 043844.
Jaynes, E., and F. W. Cummings, 1963, Proc. IEEE **51**, 89.
Jelezko, F., T. Gaebel, I. Popa, M. Domhan, A. Gruber, and J. Wrachtrup, 2004, Phys. Rev. Lett. **93**, 130501.
Jobez, P., I. Usmani, N. Timoney, C. Laplane, N. Gisin, and M. Afzelius, 2014, New J. Phys. **16**, 083005.
Junge, C., D. O'Shea, J. Volz, and A. Rauschenbeutel, 2013, Phys. Rev. Lett. **110**, 213604.
Kalb, N., P. C. Humphreys, J. J. Slim, and R. Hanson, 2018, Phys. Rev. A **97**, 062330.
Kalb, N., A. Reiserer, S. Ritter, and G. Rempe, 2015, Phys. Rev. Lett. **114**, 220501.
Kalb, N., A. A. Reiserer, P. C. Humphreys, J. J. W. Bakermans, S. J. Kamerling, N. H. Nickerson, S. C. Benjamin, D. J. Twitchen, M. Markham, and R. Hanson, 2017, Science **356**, 928.
Kastoryano, M. J., F. Reiter, and A. S. Sørensen, 2011, Phys. Rev. Lett. **106**, 090502.
Kaupp, H., T. Hümmer, M. Mader, B. Schlederer, J. Benedikter, P. Haeusser, H.-C. Chang, H. Fedder, T. W. Hänsch, and D. Hunger, 2016, Phys. Rev. Applied **6**, 054010.
Khabiboulline, E. T., J. Borregaard, K. De Greve, and M. D. Lukin, 2019, Phys. Rev. Lett. **123**, 070504.
Kimble, H. J., 2008, Nature (London) **453**, 1023.
Kindem, J. M., A. Ruskuc, J. G. Bartholomew, J. Rochman, Y. Q. Huan, and A. Faraon, 2020, Nature (London) **580**, 201.
Kinos, A., *et al.*, 2021, arXiv:2103.15743.
Kleppner, D., 1981, Phys. Rev. Lett. **47**, 233.
Knill, E., R. Laflamme, and G. J. Milburn, 2001, Nature (London) **409**, 46.
Kolesov, R., K. Xia, R. Reuter, R. Stöhr, A. Zappe, J. Meijer, P. R. Hemmer, and J. Wrachtrup, 2012, Nat. Commun. **3**, 1029.
Kómár, P., E. M. Kessler, M. Bishof, L. Jiang, A. S. Sørensen, J. Ye, and M. D. Lukin, 2014, Nat. Phys. **10**, 582.
Kono, S., K. Koshino, Y. Tabuchi, A. Noguchi, and Y. Nakamura, 2018, Nat. Phys. **14**, 546.
Körber, M., O. Morin, S. Langenfeld, A. Neuzner, S. Ritter, and G. Rempe, 2018, Nat. Photonics **12**, 18.
Kornher, T., D.-W. Xiao, K. Xia, F. Sardi, N. Zhao, R. Kolesov, and J. Wrachtrup, 2020, Phys. Rev. Lett. **124**, 170402.
Kuhn, A., M. Hennrich, T. Bondo, and G. Rempe, 1999, Appl. Phys. B **69**, 373.
Kutluer, K., M. Mazzera, and H. de Riedmatten, 2017, Phys. Rev. Lett. **118**, 210502.
Lago-Rivera, D., S. Grandi, J. V. Rakonjac, A. Seri, and H. de Riedmatten, 2021, Nature (London) **594**, 37.
Lamata, L., D. R. Leibrandt, I. L. Chuang, J. I. Cirac, M. D. Lukin, V. Vuletić, and S. F. Yelin, 2011, Phys. Rev. Lett. **107**, 030501.

Langenfeld, S., O. Morin, M. Körber, and G. Rempe, 2020, npj Quantum Inf. **6**, 86.

Langenfeld, S., P. Thomas, O. Morin, and G. Rempe, 2021, Phys. Rev. Lett. **126**, 230506.

Langenfeld, S., S. Welte, L. Hartung, S. Daiss, P. Thomas, O. Morin, E. Distante, and G. Rempe, 2021, Phys. Rev. Lett. **126**, 130502.

Langer, C., *et al.*, 2005, Phys. Rev. Lett. **95**, 060502.

Laplane, C., P. Jobez, J. Etesse, N. Gisin, and M. Afzelius, 2017, Phys. Rev. Lett. **118**, 210501.

Leibfried, D., R. Blatt, C. Monroe, and D. Wineland, 2003, Rev. Mod. Phys. **75**, 281.

Leuchs, G., and M. Sondermann, 2013, J. Mod. Opt. **60**, 36.

Levonian, D. S., R. Riedinger, B. Machielse, E. N. Knall, M. K. Bhaskar, C. M. Knaut, R. Bekenstein, H. Park, M. Lončar, and M. D. Lukin, 2022, Phys. Rev. Lett. **128**, 213602.

Lidar, D. A., and T. A. Brun, 2013, *Quantum Error Correction* (Cambridge University Press, Cambridge, England).

Lines, M. E., 1984, Science **226**, 663.

Liu, G., and B. Jacquier, 2005, Eds., *Spectroscopic Properties of Rare Earths in Optical Materials* (Springer-Verlag, Berlin).

Liu, H.-Y., *et al.*, 2020, Natl. Sci. Rev. **7**, 921.

Lodahl, P., S. Mahmoodian, and S. Stobbe, 2015, Rev. Mod. Phys. **87**, 347.

Lodahl, P., S. Mahmoodian, S. Stobbe, A. Rauschenbeutel, P. Schneeweiss, J. Volz, H. Pichler, and P. Zoller, 2017, Nature (London) **541**, 473.

Lu, H., F. Issam Baida, G. Ulliac, N. Courjal, M. Collet, and M.-P. Bernal, 2012, Appl. Phys. Lett. **101**, 151117.

Lukin, D. M., M. A. Guidry, and J. Vučković, 2020, PRX Quantum **1**, 020102.

Lütkenhaus, N., J. Calsamiglia, and K.-A. Suominen, 1999, Phys. Rev. A **59**, 3295.

Lvovsky, A. I., B. C. Sanders, and W. Tittel, 2009, Nat. Photonics **3**, 706.

Macfarlane, R. M., 2007, J. Lumin. **125**, 156.

Madjarov, I. S., J. P. Covey, A. L. Shaw, J. Choi, A. Kale, A. Cooper, H. Pichler, V. Schkolnik, J. R. Williams, and M. Endres, 2020, Nat. Phys. **16**, 857.

Maring, N., P. Farrera, K. Kutluer, M. Mazzera, G. Heinze, and H. de Riedmatten, 2017, Nature (London) **551**, 485.

Maurer, P. C., *et al.*, 2012, Science **336**, 1283.

Mazzocchi, V., P. G. Sennikov, A. D. Bulanov, M. F. Churbanov, B. Bertrand, L. Hutin, J. P. Barnes, M. N. Drozdov, J. M. Hartmann, and M. Sanquer, 2019, J. Cryst. Growth **509**, 1.

Menon, S. G., K. Singh, J. Borregaard, and H. Bernien, 2020, New J. Phys. **22**, 073033.

Merkel, B., 2021, Ph.D. thesis (Technische Universität München).

Merkel, B., P. Cova Fariña, and A. Reiserer, 2021, Phys. Rev. Lett. **127**, 030501.

Merkel, B., A. Ulanowski, and A. Reiserer, 2020, Phys. Rev. X **10**, 041025.

Moehring, D. L., P. Maunz, S. Olmschenk, K. C. Younge, D. N. Matsukevich, L.-M. Duan, and C. Monroe, 2007, Nature (London) **449**, 68.

Monroe, C., and J. Kim, 2013, Science **339**, 1164.

Morin, O., M. Körber, S. Langenfeld, and G. Rempe, 2019, Phys. Rev. Lett. **123**, 133602.

Morioka, N., *et al.*, 2020, Nat. Commun. **11**, 2516.

Mosor, S., J. Hendrickson, B. C. Richards, J. Sweet, G. Khitrova, H. M. Gibbs, T. Yoshie, A. Scherer, O. B. Shchekin, and D. G. Deppe, 2005, Appl. Phys. Lett. **87**, 141105.

Mücke, M., J. Bochmann, C. Hahn, A. Neuzner, C. Nölleke, A. Reiserer, G. Rempe, and S. Ritter, 2013, Phys. Rev. A **87**, 063805.

Munro, W. J., A. M. Stephens, S. J. Devitt, K. A. Harrison, and K. Nemoto, 2012, Nat. Photonics **6**, 777.

Muralidharan, S., L. Li, J. Kim, N. Lütkenhaus, M. D. Lukin, and L. Jiang, 2016, Sci. Rep. **6**, 20463.

Nagy, R., *et al.*, 2019, Nat. Commun. **10**, 1954.

Najer, D., *et al.*, 2019, Nature (London) **575**, 622.

Negnevitsky, V., M. Marinelli, K. K. Mehta, H.-Y. Lo, C. Flühmann, and J. P. Home, 2018, Nature (London) **563**, 527.

Neumann, P., *et al.*, 2010, Nat. Phys. **6**, 249.

Neuzner, A., M. Körber, O. Morin, S. Ritter, and G. Rempe, 2016, Nat. Photonics **10**, 303.

Nguyen, C. T., *et al.*, 2019, Phys. Rev. Lett. **123**, 183602.

Nickerson, N. H., Y. Li, and S. C. Benjamin, 2013, Nat. Commun. **4**, 1756.

Niemietz, D., P. Farrera, S. Langenfeld, and G. Rempe, 2021, Nature (London) **591**, 570.

Nölleke, C., A. Neuzner, A. Reiserer, C. Hahn, G. Rempe, and S. Ritter, 2013, Phys. Rev. Lett. **110**, 140403.

Ortu, A., A. Tiranov, S. Welinski, F. Fröwis, N. Gisin, A. Ferrier, P. Goldner, and M. Afzelius, 2018, Nat. Mater. **17**, 671.

Pfaff, W., *et al.*, 2014, Science **345**, 532.

Phenicie, C. M., P. Stevenson, S. Welinski, B. C. Rose, A. T. Asfaw, R. J. Cava, S. A. Lyon, N. P. de Leon, and J. D. Thompson, 2019, Nano Lett. **19**, 8928.

Pikovski, I., M. Zych, F. Costa, and Č. Brukner, 2015, Nat. Phys. **11**, 668.

Pöllinger, M., D. O'Shea, F. Warken, and A. Rauschenbeutel, 2009, Phys. Rev. Lett. **103**, 053901.

Pompili, M., *et al.*, 2021, Science **372**, 259.

Preskill, J., 2018, Quantum **2**, 79.

Probst, S., H. Rotzinger, A. V. Ustinov, and P. A. Bushev, 2015, Phys. Rev. B **92**, 014421.

Proctor, T. J., P. A. Knott, and J. A. Dunningham, 2018, Phys. Rev. Lett. **120**, 080501.

Purcell, E. M., 1946, Phys. Rev. **69**, 37.

Raha, M., S. Chen, C. M. Phenicie, S. Ourari, A. M. Dibos, and J. D. Thompson, 2020, Nat. Commun. **11**, 1605.

Rakonjac, J. V., Y.-H. Chen, S. P. Horvath, and J. J. Longdell, 2020, Phys. Rev. B **101**, 184430.

Rančić, M., M. P. Hedges, R. L. Ahlefeldt, and M. J. Sellars, 2018, Nat. Phys. **14**, 50.

Reiserer, A., N. Kalb, M. S. Blok, K. J. M. van Bemmelen, T. H. Taminiau, R. Hanson, D. J. Twitchen, and M. Markham, 2016, Phys. Rev. X **6**, 021040.

Reiserer, A., N. Kalb, G. Rempe, and S. Ritter, 2014, Nature (London) **508**, 237.

Reiserer, A., C. Nölleke, S. Ritter, and G. Rempe, 2013, Phys. Rev. Lett. **110**, 223003.

Reiserer, A., and G. Rempe, 2015, Rev. Mod. Phys. **87**, 1379.

Reiserer, A., S. Ritter, and G. Rempe, 2013, Science **342**, 1349.

Rempe, G., R. Lalezari, R. J. Thompson, and H. J. Kimble, 1992, Opt. Lett. **17**, 363.

Riedel, D., F. Fuchs, H. Kraus, S. Väth, A. Sperlich, V. Dyakonov, A. A. Soltamova, P. G. Baranov, V. A. Ilyin, and G. V. Astakhov, 2012, Phys. Rev. Lett. **109**, 226402.

Riedel, D., I. Söllner, B. J. Shields, S. Starosielec, P. Appel, E. Neu, P. Maletinsky, and R. J. Warburton, 2017, Phys. Rev. X **7**, 031040.

Riedinger, R., A. Wallucks, I. Marinković, C. Löschnauer, M. Aspelmeyer, S. Hong, and S. Gröblacher, 2018, Nature (London) **556**, 473.

Ritter, S., C. Nölleke, C. Hahn, A. Reiserer, A. Neuzner, M. Uphoff, M. Mücke, E. Figueroa, J. Bochmann, and G. Rempe, 2012, Nature (London) **484**, 195.

Robledo, L., L. Childress, H. Bernien, B. Hensen, P. F. A. Alkemade, and R. Hanson, 2011, Nature (London) **477**, 574.

Rogers, L. J., *et al.*, 2014, Phys. Rev. Lett. **113**, 263602.

Rose, B. C., *et al.*, 2018, Science **361**, 60.

Rozpedek, F., K. Goodenough, J. Ribeiro, N. Kalb, V. C. Vivoli, A. Reiserer, R. Hanson, S. Wehner, and D. Elkouss, 2018, Quantum Sci. Technol. **3**, 034002.

Rugar, A. E., S. Aghaeimeibodi, D. Riedel, C. Dory, H. Lu, P. J. McQuade, Z.-X. Shen, N. A. Melosh, and J. Vučković, 2021, Phys. Rev. X **11**, 031021.

Ruskuc, A., C.-J. Wu, J. Rochman, J. Choi, and A. Faraon, 2022, Nature (London) **602**, 408.

Sabooni, M., Q. Li, S. Kröll, and L. Rippe, 2013, Phys. Rev. Lett. **110**, 133604.

Saffman, M., T. G. Walker, and K. Mølmer, 2010, Rev. Mod. Phys. **82**, 2313.

Saglamyurek, E., N. Sinclair, J. Jin, J. A. Slater, D. Oblak, F. Bussières, M. George, R. Ricken, W. Sohler, and W. Tittel, 2011, Nature (London) **469**, 512.

Samutpraphoot, P., T. Đorđević, P. L. Ocola, H. Bernien, C. Senko, V. Vuletić, and M. D. Lukin, 2020, Phys. Rev. Lett. **124**, 063602.

Sangouard, N., C. Simon, H. de Riedmatten, and N. Gisin, 2011, Rev. Mod. Phys. **83**, 33.

Santori, C., *et al.*, 2006, Phys. Rev. Lett. **97**, 247401.

Scheucher, M., A. Hilico, E. Will, J. Volz, and A. Rauschenbeutel, 2016, Science **354**, 1577.

Seri, A., A. Lenhard, D. Rieländer, M. Gündoğan, P. M. Ledingham, M. Mazzera, and H. de Riedmatten, 2017, Phys. Rev. X **7**, 021028.

Shomroni, I., S. Rosenblum, Y. Lovsky, O. Bechler, G. Guendelman, and B. Dayan, 2014, Science **345**, 903.

Simon, C., H. de Riedmatten, M. Afzelius, N. Sangouard, H. Zbinden, and N. Gisin, 2007, Phys. Rev. Lett. **98**, 190503.

Simon, J., H. Tanji, S. Ghosh, and V. Vuletić, 2007, Nat. Phys. **3**, 765.

Simon, J., H. Tanji, J. K. Thompson, and V. Vuletić, 2007, Phys. Rev. Lett. **98**, 183601.

Sinclair, N., *et al.*, 2014, Phys. Rev. Lett. **113**, 053603.

Sipahigil, A., M. L. Goldman, E. Togan, Y. Chu, M. Markham, D. J. Twitchen, A. S. Zibrov, A. Kubanek, and M. D. Lukin, 2012, Phys. Rev. Lett. **108**, 143601.

Sipahigil, A., K. D. Jahnke, L. J. Rogers, T. Teraji, J. Isoya, A. S. Zibrov, F. Jelezko, and M. D. Lukin, 2014, Phys. Rev. Lett. **113**, 113602.

Sipahigil, A., *et al.*, 2016, Science **354**, 847.

Siyushev, P., H. Pinto, M. Vörös, A. Gali, F. Jelezko, and J. Wrachtrup, 2013, Phys. Rev. Lett. **110**, 167402.

Slattery, O. T., L. Ma, K. Zong, and X. Tang, 2019, J. Res. Natl. Inst. Stand. Technol. **124**, 124019.

Sørensen, A. S., and K. Mølmer, 2003, Phys. Rev. Lett. **91**, 097905.

Specht, H. P., C. Nölleke, A. Reiserer, M. Uphoff, E. Figueroa, S. Ritter, and G. Rempe, 2011, Nature (London) **473**, 190.

Stas, P.-J., *et al.*, 2022, arXiv:2207.13128.

Stephenson, L. J., D. P. Nadlinger, B. C. Nichol, S. An, P. Drmota, T. G. Ballance, K. Thirumalai, J. F. Goodwin, D. M. Lucas, and C. J. Ballance, 2020, Phys. Rev. Lett. **124**, 110501.

Stevenson, P., *et al.*, 2022, Phys. Rev. B **105**, 224106.

Stolz, T., H. Hegels, M. Winter, B. Röhr, Y.-F. Hsiao, L. Husel, G. Rempe, and S. Dürr, 2022, Phys. Rev. X **12**, 021035.

Sukachev, D. D., A. Sipahigil, C. T. Nguyen, M. K. Bhaskar, R. E. Evans, F. Jelezko, and M. D. Lukin, 2017, Phys. Rev. Lett. **119**, 223602.

Sun, S., H. Kim, Z. Luo, G. S. Solomon, and E. Waks, 2018, Science **361**, 57.

Suter, D., and G. A. Álvarez, 2016, Rev. Mod. Phys. **88**, 041001.

Tamarat, P., *et al.*, 2008, New J. Phys. **10**, 045004.

Taminiau, T. H., J. Cramer, T. van der Sar, V. V. Dobrovitski, and R. Hanson, 2014, Nat. Nanotechnol. **9**, 171.

Tanji, H., S. Ghosh, J. Simon, B. Bloom, and V. Vuletić, 2009, Phys. Rev. Lett. **103**, 043601.

Tanji-Suzuki, H., I. D. Leroux, M. H. Schleier-Smith, M. Cetina, A. T. Grier, J. Simon, and V. Vuletić, 2011, in *Advances In Atomic, Molecular, and Optical Physics*, Vol. 60, edited by E. Arimondo, P. R. Berman, and C. C. Lin (Academic Press, New York), pp. 201–237.

Tchebotareva, A., *et al.*, 2019, Phys. Rev. Lett. **123**, 063601.

Thiel, C. W., T. Böttger, and R. L. Cone, 2011, J. Lumin. **131**, 353.

Thompson, J. K., J. Simon, H. Loh, and V. Vuletić, 2006, Science **313**, 74.

Tiarks, D., S. Schmidt-Eberle, T. Stolz, G. Rempe, and S. Dürr, 2019, Nat. Phys. **15**, 124.

Tiecke, T. G., K. P. Nayak, J. D. Thompson, T. Peyronel, N. P. d. Leon, V. Vuletić, and M. D. Lukin, 2015, Optica **2**, 70.

Tiecke, T. G., J. D. Thompson, N. P. de Leon, L. R. Liu, V. Vuletić, and M. D. Lukin, 2014, Nature (London) **508**, 241.

Tittel, W., M. Afzelius, T. Chanelière, R. Cone, S. Kröll, S. Moiseev, and M. Sellars, 2010, Laser Photonics Rev. **4**, 244.

Togan, E., *et al.*, 2010, Nature (London) **466**, 730.

Trusheim, M. E., *et al.*, 2020, Phys. Rev. Lett. **124**, 023602.

Ulanowski, A., B. Merkel, and A. Reiserer, 2022, Sci. Adv. **8**, eabo4538.

Uphoff, M., M. Brekenfeld, G. Rempe, and S. Ritter, 2016, Appl. Phys. B **122**, 46.

Usmani, I., M. Afzelius, H. de Riedmatten, and N. Gisin, 2010, Nat. Commun. **1**, 12.

Utikal, T., E. Eichhammer, L. Petersen, A. Renn, S. Götzinger, and V. Sandoghdar, 2014, Nat. Commun. **5**, 3627.

Vahala, K. J., 2003, Nature (London) **424**, 839.

Vandersypen, L. M. K., and I. L. Chuang, 2005, Rev. Mod. Phys. **76**, 1037.

van Leent, T., M. Bock, R. Garthoff, K. Redeker, W. Zhang, T. Bauer, W. Rosenfeld, C. Becher, and H. Weinfurter, 2020, Phys. Rev. Lett. **124**, 010510.

Vetsch, E., D. Reitz, G. Sagué, R. Schmidt, S. T. Dawkins, and A. Rauschenbeutel, 2010, Phys. Rev. Lett. **104**, 203603.

Vivien, L., and L. Pavesi, 2013, *Handbook of Silicon Photonics* (Taylor & Francis, London).

Volz, J., R. Gehr, G. Dubois, J. Estève, and J. Reichel, 2011, Nature (London) **475**, 210.

Volz, J., M. Scheucher, C. Junge, and A. Rauschenbeutel, 2014, Nat. Photonics **8**, 965.

Wachter, G., *et al.*, 2019, Light Sci. Appl. **8**, 37.

Waldherr, G., *et al.*, 2014, Nature (London) **506**, 204.

Wallucks, A., I. Marinković, B. Hensen, R. Stockill, and S. Gröblacher, 2020, Nat. Phys. **16**, 772.

Wan, N. H., *et al.*, 2020, Nature (London) **583**, 226.

Wang, D., H. Kelkar, D. Martin-Cano, D. Rattenbacher, A. Shkarin, T. Utikal, S. Götzinger, and V. Sandoghdar, 2019, Nat. Phys. **15**, 483.

Wang, J., F. Sciarrino, A. Laing, and M. G. Thompson, 2020, Nat. Photonics **14**, 273.

Wang, J.-F., *et al.*, 2020, Phys. Rev. Lett. **124**, 223601.

Wang, P., C.-Y. Luan, M. Qiao, M. Um, J. Zhang, Y. Wang, X. Yuan, M. Gu, J. Zhang, and K. Kim, 2021, Nat. Commun. **12**, 233.

Wehner, S., D. Elkouss, and R. Hanson, 2018, Science **362**, eaam9288.

Weiss, L., A. Gritsch, B. Merkel, and A. Reiserer, 2021, Optica **8**, 40.

Welte, S., B. Hacker, S. Daiss, S. Ritter, and G. Rempe, 2018, Phys. Rev. X **8**, 011018.

Werschnik, J., and E. K. U. Gross, 2007, J. Phys. B **40**, R175.
Wilk, T., A. Gaetan, C. Evellin, J. Wolters, Y. Miroshnychenko, P. Grangier, and A. Browaeys, 2010, Phys. Rev. Lett. **104**, 010502.
Williamson, L. A., and J. J. Longdell, 2014, New J. Phys. **16**, 073046.
Wolfowicz, G., C. P. Anderson, B. Diler, O. G. Poluektov, F. J. Heremans, and D. D. Awschalom, 2020, Sci. Adv. **6**, eaaz1192.
Wolfowicz, G., F. J. Heremans, C. P. Anderson, S. Kanai, H. Seo, A. Gali, G. Galli, and D. D. Awschalom, 2021, Nat. Rev. Mater. **6**, 906.
Xia, K., F. Sardi, C. Sauerzapf, T. Kornher, H.-W. Becker, Z. Kis, L. Kovacs, R. Kolesov, and J. Wrachtrup, 2022, Optica **9**, 445.
Yale, C. G., B. B. Buckley, D. J. Christle, G. Burkard, F. J. Heremans, L. C. Bassett, and D. D. Awschalom, 2013, Proc. Natl. Acad. Sci. U.S.A. **110**, 7595.
Yin, C., M. Rancic, G. G. de Boo, N. Stavrias, J. C. McCallum, M. J. Sellars, and S. Rogge, 2013, Nature (London) **497**, 91.
Yin, J., *et al.*, 2017, Science **356**, 1140.
Yu, Y., *et al.*, 2020, Nature (London) **578**, 240.
Zaske, S., *et al.*, 2012, Phys. Rev. Lett. **109**, 147404.
Zhang, C., Y.-F. Huang, B.-H. Liu, C.-F. Li, and G.-C. Guo, 2021, Adv. Quantum Technol. **4**, 2000132.
Zhong, M., M. P. Hedges, R. L. Ahlefeldt, J. G. Bartholomew, S. E. Beavan, S. M. Wittig, J. J. Longdell, and M. J. Sellars, 2015, Nature (London) **517**, 177.
Zhong, T., and P. Goldner, 2019, Nanophotonics **8**, 2003.
Zhong, T., *et al.*, 2017, Science **357**, 1392.
Zhong, T., *et al.*, 2018, Phys. Rev. Lett. **121**, 183603.
Żukowski, M., A. Zeilinger, M. A. Horne, and A. K. Ekert, 1993, Phys. Rev. Lett. **71**, 4287.